Tobramycin liquid crystal nanoparticles eradicate cystic fibrosis-related *Pseudomonas aeruginosa* biofilms

Chelsea R. Thorn [A,B,C], *Cristiane de Souza Carvalho-Wodarz* [E], *Justus C. Horstmann* [E,F], *Claus-Michael Lehr* [E,F], *Clive A. Prestidge* [A,C] *and Nicky Thomas* [A,B,C,D]*

A. University of South Australia, Clinical and Health Science, North Tce, Adelaide, SA 5000, Australia

B. The Basil Hetzel Institute for Translational Health Research, Woodville, SA 5011, Australia

C. ARC Centre for Excellence in Bio-Nano Science and Technology, Australia

D. Biofilm Test Facility, Cancer Research Institute, University of South Australia, North Tce, Adelaide, SA 5000, Australia

E. Helmholtz Institute for Pharmaceutical Research Saarland (HIPS), 66123 Saarbrücken, Germany.

F. Department of Pharmacy, Saarland University, 66123 Saarbrücken, Germany.

Keywords: Antimicrobials, pulmonary drug delivery, lung infection co-cultures, biofilms, cystic fibrosis, liquid crystals

Pseudomonas aeruginosa biofilms cause persistent and chronic infections, most known clinically in cystic fibrosis. Tobramycin is a standard anti-pseudomonal antibiotic; however, in biofilm infections, its efficacy severely decreases due to limited permeability across the biofilm matrix. Herewith, we discover a biomimetic, nanostructured, lipid liquid crystal nanoparticle-(LCNPs)-based material for tobramycin that significantly enhances the efficacy of tobramycin and eradicates *P. aeruginosa* biofilm infection. Using an advanced, biologically-relevant co-

culture model of human cystic fibrosis bronchial epithelial cells infected with *P. aeruginosa* biofilms at an air-liquid interface, nebulized tobramycin-LCNPs completely eradicated 1 x 10^9 CFU/mL of *P. aeruginosa* after two doses, a 100-fold improvement over the unformulated antibiotic. The enhanced activity of tobramycin was not observed with a liposomal formulation of tobramycin or with ciprofloxacin, an antibiotic that readily penetrates biofilms. We demonstrate that the unique nanostructure of the LCNPs drives the enhanced penetration of tobramycin across the biofilm barrier, but not through the healthy lung epithelium barrier, significantly increasing the available antibiotic concentration at the site of infection. The LCNPs are an innovative strategy to improve the performance of tobramycin as a directed pulmonary therapy, enabling the administration of lower doses, reducing the toxicity and amplifying the anti-biofilm activity of the anti-pseudomonal antibiotic.

1. Introduction

Bacterial biofilms are notorious for forming insidious, persistent and chronic infections that prevail in up to 65-80% of all bacterial infections.[1] Biofilms are a dense community of bacteria surrounded by a thick matrix of extracellular polymeric substances (EPS).[2] With tightly regulated communication through quorum sensing and the protective matrix, biofilms can tolerate up to 1000-fold higher concentrations of antibiotics. *Pseudomonas aeruginosa* is a ubiquitous opportunistic pathogen that consistently survives as a biofilm within the lungs of cystic fibrosis (CF) patients.[3] CF is an inheritable autosomal disease characterized by a mutation in the CF transmembrane regulation (CFTR) protein, resulting in dysfunctional salt transport across epithelial surfaces and the accumulation of thick, viscous mucus in the lungs and digestive tract, which are ideal breeding grounds for bacteria.[4] Coupled with the obstacle of clearing the continually produced viscous mucus, eradicating and preventing *P. aeruginosa* biofilm colonization is a momentous global healthcare challenge.

Aminoglycosides are standard antipseudomonal therapy for *P. aeruginosa* lung infections in CF, administered twice daily via inhalation at monthly intervals.[5] Therapy is life long, and the goal is at present limited to managing the bacterial load rather than eradicating the bacteria.[6] Tobramycin is of limited effectivity against *P. aeruginosa* biofilms due to the inability of the antibiotic to penetrate the biofilm and the presence of the thick mucus.[7, 8] As a cationic molecule, tobramycin is bound to the various negatively charged polysaccharides of the biofilm matrix, unable to reach the inner community of bacteria.[9] Tobramycin elicits its antimicrobial effect by inhibiting protein synthesis and causing cell membrane damage. It is a concentration-dependent antibiotic, therefore achieving a sufficiently high concentration is critical.[10] Due to this requirement, the extensive tobramycin regimen often results in increased cases of irreversible nephro- and ototoxicity in patients.[11] Other antibiotics, such as ciprofloxacin, are also employed in the treatment of *P. aeruginosa* in CF. In contrast to tobramycin, ciprofloxacin can penetrate the EPS. However, due to the low metabolic activity of bacteria, the antimicrobial effect of ciprofloxacin via inhibition of DNA synthesis is limited.[9]

Drug delivery systems and nanotechnology have been of considerable interest to overcome challenging barriers in biofilm infections.[12, 13] Local administration by oral inhalation directly to the lungs may be expected to conceal the antibiotic charge and improve the penetration into the biofilm matrix. Liposomal formulations have been the most popular and successful strategy due to their potential to fuse with bacterial cell membranes, facilitating a targeted action and increasing the concentration of antibiotic in the bacterial cell.[14] Recently, the US Food and Drug Administration approved Arikayce®, an inhalable liposomal formulation of amikacin for *Mycobacteria avium* complex lung infection.[15, 16] In addition to the fusogenic properties, the sub-micron size and surface properties of liposomes enhance the delivery of antibiotics directly to the site of infection while also improving aminoglycoside penetration in biofilm and intracellular type bacterial infections.

Liposomes comprise of a phospholipid lamellar bilayer surrounding an aqueous cavity for loading hydrophilic and amphiphilic drugs, while the lipid bilayer can house lipophilic drugs.[17] Lipids can further self-assemble into higher-ordered non-lamellar structures, with increased curvature of the lipid bilayer to form 3D mesophases such as the bicontinuous cubic and inverse hexagonal.[18, 19] These are broadly termed liquid crystals and are of interest for drug delivery due to offering a greater internal surface area of the lipid bilayer with the ability to load more amphiphilic, hydrophilic and lipophilic drugs.[20, 21] Monoolein (MO) and phytantriol (PHY) are the most commonly used lipids to form liquid crystals.[22-24] Dispersion of the liquid crystals in a surfactant forms liquid crystal nanoparticles (LCNPs) which are also known as cubosomes and hexasomes, based on the liquid crystal mesophase. We have recently established LCNPs as a drug delivery system for a range of antimicrobials, where the drug release is triggered by the presence of bacteria. Specifically, bacteria-produced lipases were shown to digest the liquid crystal structure, releasing encapsulated antibiotics.[25] We hypothesized that the larger lipid bilayer surface area and unique nanostructure of LCNPs would improve the penetration of tobramycin through biofilms and impart enhanced antimicrobial efficacy.

Accurate and reliable *in vivo* models of lungs infected with *P. aeruginosa* biofilms to evaluate novel antimicrobial therapies are difficult to achieve, where next to none exist.[26] *In vitro* cell cultures can provide valuable, reproducible and biologically-relevant information that complies with humane experimental techniques.[27-29] Recently, a sophisticated and advanced *in vitro* cell co-culture model based on human bronchial epithelial cells (CFBE41o-) with *P. aeruginosa* biofilms was developed by Horstmann *et al*. [manuscript in preparation]. The CFBE41o- cell line, derived from patients with the CFTR mutation are cultured at the air-liquid interface in Transwell® inserts and mimic the environment of the lung's conducting zone. After the cells form a tight barrier, a pre-formed, three-day old biofilm is transferred on to the cell monolayer. *P. aeruginosa* forms micro-(biofilm)-colonies on top of the CFBE41o- cell layer that are

visually equivalent to the pathology observed in the lungs of *P. aeruginosa* infected cystic fibrosis patients.[30] The infection can be maintained for several days with repeated aerosolized treatments, modelling chronic pulmonary infections with relevant cellular and non-cellular barriers that are usually not replicated in other, more simplified *in vitro* models. Uniquely, the chronic infection model combines the effect of bacteria and the host cell inflammatory response, providing a more accurate, up-scalable and high throughput model of the infected cystic fibrosis bronchial epithelium, reducing the need to use animals.

Here we describe LCNPs as a pulmonary drug delivery system for tobramycin using various biofilm models of infections and compare to the unformulated antibiotic and liposomes. We showcase and contrast the effect of tobramycin LCNPs in simple *in vitro* models, advanced flow cell and *in vitro* infected cell co-culture models mimicking CF-related *P. aeruginosa* biofilm lung infections in pulmonary bronchial epithelial cell monolayers. Throughout, we establish tobramycin LCNPs as an advanced pulmonary drug delivery system and elucidate the mechanisms for advancing the efficacy of tobramycin.

2. Results and Discussion

2.1. Tobramycin loaded LCNPs: loading, release and nebulization

Tobramycin (TOB) loaded LCNPs were formed with well-defined particle sizes of 170 nm and 200 nm for MO- and PHY, respectively. PHY-LCNPs were notably less stable than MO-LCNPs, often separating from the suspension and required constant dispersion via bath sonication before use. Both LCNPs carried a slightly negative surface charge and an encapsulation efficiency of ~85%, with a TOB loading between 21 and 25 % w/w. Liposomes with comparable particle size and decreased zeta potential were also formed, along with LCNPs stabilized with varying amounts of polyethylene oxide (PEO-)- polypropylene oxide (PPO)-PEO, as shown in **Figure 1A**. Previously, MO- and PHY-LCNPs containing no drug and small molecule hydrophilic

antibiotics (i.e. ciprofloxacin) had an inverse hexagonal liquid crystal phase structure that upon dilution (i.e. in media for release and activity assessment) switched to the bicontinuous cubic phase structure [25]. The structural unit of the TOB LCNPs is equivalent due to its molecular size and hydrophilicity and is structurally demonstrated in the schematic in **Figure 1**D. In comparison, the simplistic structure of liposomes is shown schematically in **Figure 1**E

TOB was released rapidly from the LCNPs within two hours, in line with our previous reports on ciprofloxacin (CIP) loaded LCNPs.[25] The rate of TOB released from the MO-LCNPs was initially higher compared to PHY-LCNPs; however, it became equivalent after the plateau. According to Higuchi,[31] the matrix of the lipid's liquid crystal structure controls the release of the loaded antibiotics by diffusion. The rate of TOB released from MO- and PHY-LCNPs were 208 µg/min$^{1/2}$ and 272 µg/min$^{1/2}$, respectively, and at least 5-fold higher compared to the release from the liposomes. As shown previously, liposomes are known to retain a higher amount of small, hydrophilic molecules, where 80% of TOB remained within the aqueous core.[32] LCNPs are three-dimensional constructs of multiple lipid bilayers, where the water channels remain exposed to the outer medium, unlike the single lipid bilayer of liposomes that fully encloses the inner aqueous compartment. Thus, due to the configuration of the lipid nanoparticles, the rapid release of TOB from LCNPs was expected. We have previously shown MO-LCNPs respond to bacterial lipase, triggering the release of loaded large molecular weight and hydrophobic antimicrobials.[25] Due to the low molecular weight and hydrophilic nature of TOB and CIP, the diffusion-controlled release from the aqueous channels is rapid and would co-occur with the bacterial lipase digestion the LCNPs crystalline structure.

A.

Formulations	Particle size (nm)	PDI	Zeta Potential (mV)	TOB loaded (% w/w)	Release rate (μg/min$^{1/2}$)
Phytantriol (PHY)-LCNPs	313 ± 6	0.56 ± 0.03	-11.2 ± 1.0	21	272
Monoolein (MO) (0.3% w/v Pluronic® F-127)	164 ± 2	0.16 ± 0.01	-10.4 ± 0.4	25	208
MO-LCNPs (5% w/v Pluronic® F-127)	85.4 ± 1	0.17 ± 0.01	-16.1 ± 0.5	26	-
MO-LCNPs (no Pluronic® F127)	183 ± 2	0.11 ± 0.01	-10.2 ± 0.1	21	-
DSPC: DPPG liposomes	149 ± 8	0.37 ± 0.01	-43.5 ± 0.1	3	42

B.

C.

TOB formulations	Particle size (nm)	PDI	Zeta potential (mV)	Total Mass Deposited (μg)
Unformulated	-	-	-	10.8 ± 0.3
PHY-LCNPs	247 ± 1	0.32 ± 0.01	-1.1 ± 0.1	10.4 ± 0.2
MO-LCNPs	199 ± 3	0.37 ± 0.01	-2.1 ± 0.1	13.5 ± 0.4

D.

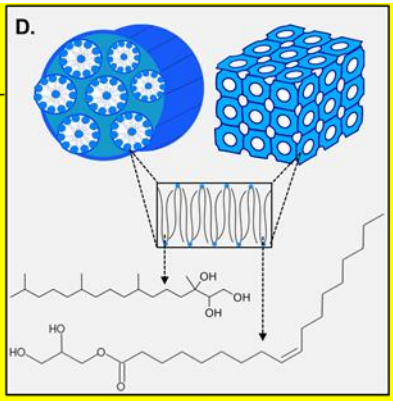

E.

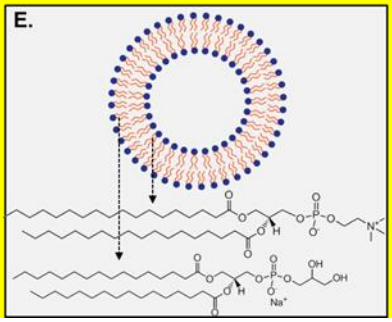

***Figure 1**. Tobramycin formulation characteristics A. The particle size, zeta potential, tobramycin load and release rate in 50 – 150 mM Tris – NaCl buffer, pH 7.4 of various LCNPs and liposomes. B. The nebulization set up using the Aerogen® Pro (vibrating mesh nebulizer) and deposition device, fitted into wells of a 24 well plate, as described by Horstmann et al.[33]. C. The particle size and zeta potential characteristics of LCNPs after nebulization, along with the total mass of tobramycin (TOB) deposited from nebulization of 100 μL of 3.32 mg/mL using the setup. Data represented as mean ± standard deviation, n = 9. D. Schematically represents the inverse hexagonal or bicontinuous cubic phase LCNPs and the chemical structures of phytantriol and monoolein, respectively forming the lipid bilayer. E. Schematically represents liposomes structure formed from DSPC and DPPG, respectively.*

To the best of our knowledge, LCNPs have not been reported as a pulmonary drug delivery system. Following nebulization, the LCNPs maintained their particle size, as demonstrated in **Figure 1C**. The zeta potential increased toward neutral, likely reflecting nebulization of the nanoparticles in isotonic 0.9% saline. The deposition efficiencies of TOB in an unformulated solution, MO-LCNPs and PHY-LCNPs were consistent at 3.25%, 4.05% and 3.12%, respectively. During the nebulization process, the antibiotic can be lost, e.g. by adhesion to the walls of the nebulizer and deposition device or within the vibrating mesh. Hence the low deposition efficiencies observed are not uncommon. Corresponding to the development of the straight-forward, custom-made deposition device shown in **Figure 1B,**[33] a concise and

reproducible amount of TOB was deposited from either the unformulated solution or when loaded in LCNPs.

The properties of the nanoparticle and technique of aerosol generation can cause particulate aggregation following nebulization. Previously, hydrophilic surfaces and ultrasonic nebulization decreased the aggregation of polymeric nanoparticles.[34] The LCNPs in the present study possess an overall hydrophilic surface due to the Pluronic® F-127 surface coating. While the Aerogen® nebulizer creates an aerosol through a technology vibrating the mesh at ultrasonic frequencies, limited aggregation was observed in the aerosol, similar to ultrasonic nebulizers. The limited aggregation and consistent deposition efficiencies confirm the TOB LCNP formulations can maintain their structure and action following nebulization.

2.2. LCNPs enhance the anti-biofilm activity of tobramycin, but not ciprofloxacin

The antimicrobial effect of TOB against PAO1 biofilm in the MBEC® model was enhanced significantly upon loading into LCNPs. Compared to TOB in solution and a physical mixture of drug-free LCNPs and TOB solution, TOB-loaded LCNPs reduced the load of PAO1 by 1000- and 100-fold, respectively, over a range of TOB concentrations (**Figure 2A**). The data indicated that TOB's enhanced antimicrobial effect was not due to the drug-free LCNPs but increased in a dose-responsive nature from being loaded in the MO-LCNPs.

TOB is a concentration-dependent antibiotic, where the minimum biofilm inhibitory concentration (MBIC) as an unformulated solution was 240 μg/mL in PAO1 biofilms using the MBEC® plates. The MO-LCNPs markedly reduced the MBIC of TOB to 60 – 120 μg/mL. Clinically, achieving a sufficiently high concentration of TOB at the infection site is more important than the length of time that concentration is maintained. For TOB, the maximum serum concentration to achieve a maximum therapeutic effect and minimize the risk of nephro-,

oto- and neuro-toxicity is between 12- 30 µg/mL.[35-37] However, following pulmonary administration of the commercially available TOB (TOBI Podhaler®), considerably higher sputum concentrations are achieved (i.e. 1050 µg/g) compared to limited systemic exposure with serum concentrations of 1 µg/mL.[38] In concordance, the LCNPs advanced the antimicrobial effect of TOB, significantly increasing the total reduction of bacteria at lower concentrations ($P < 0.01$).

At 5 µg/mL and 15 µg/mL, TOB MO-LCNPs reduced the PAO1 load by 100'000-fold, compared to the untreated control, while the unformulated antibiotic alone and combined with drug-free LCNPs reduced the load by 100- and 1000-fold, respectively. At the higher concentration of 60 µg/mL, TOB MO-LCNPs resulted in less than 10 CFU/mL of PAO1, which is near-complete eradication after one single treatment, with a total 100'000-fold reduction compared to the unformulated solution.

In contrast, for CIP, the antimicrobial effect could not be enhanced by loading the antibiotic into LCNPs (Figure 2**B**). As aforementioned, the CIP MO-LCNPs were previously characterized and demonstrated a similar release profile to TOB.[25] Over a range of concentrations, the antimicrobial effect of CIP in the simplified PAO1 biofilm model did not alter after loading in LCNPs, nor in the physical mixture of CIP with drug-free LCNPs (**Figure 2B**), i.e. CIP's activity was unable to be further decreased beyond 10'000 CFU/mL.

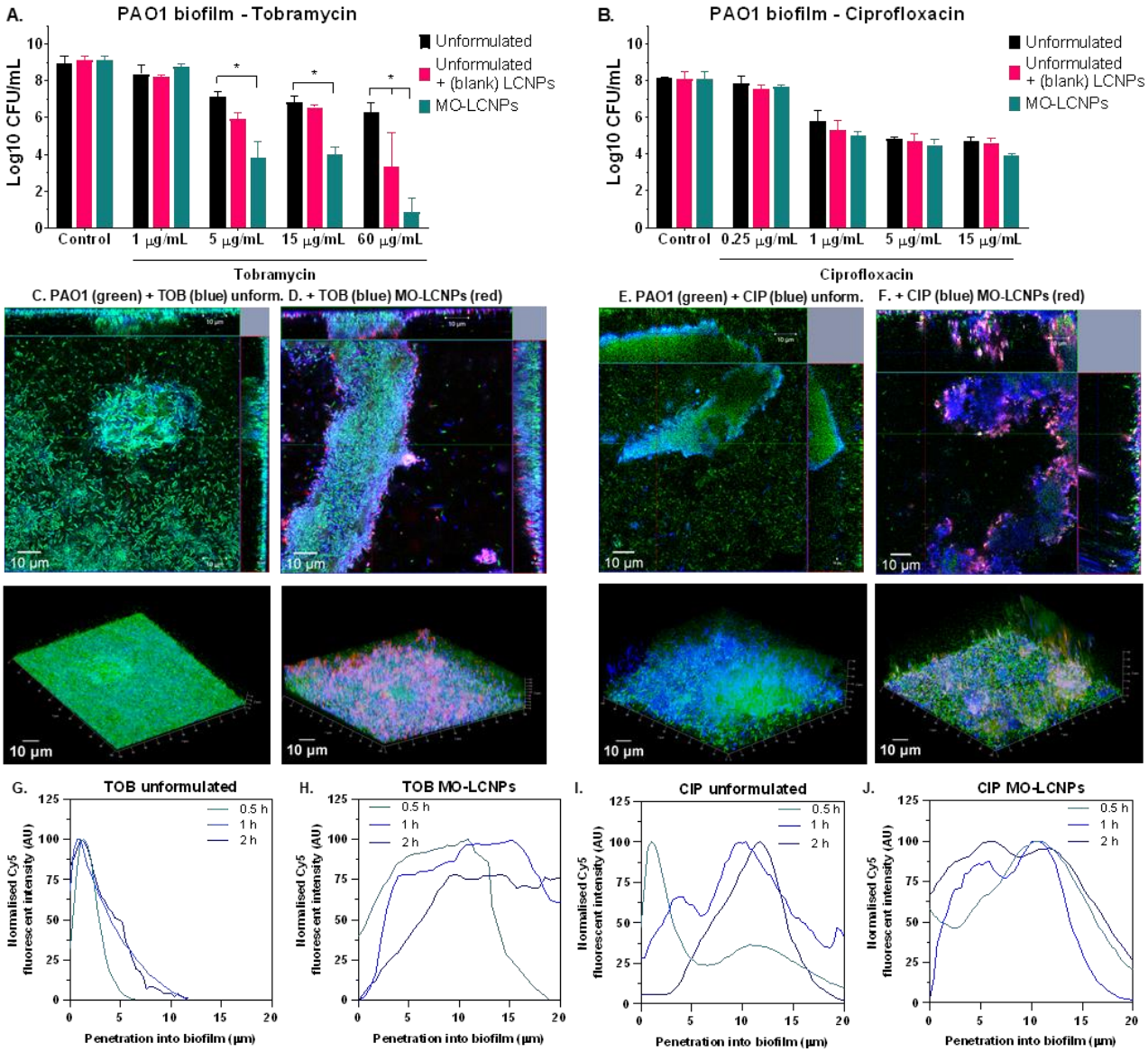

Figure 2. *Liquid crystal nanoparticles (LCNPs) enhance the antimicrobial activity of tobramycin (TOB) via enhanced biofilm penetration. The total amount of PAO1 remaining after PAO1 biofilm formed on MBEC model was treated with various concentration of A. tobramycin (TOB) and B. ciprofloxacin (CIP) as an unformulated solution (black), unformulated solution combined with drug-free MO-LCNPs (pink) and formulated as MO-LCNP (teal). Concentration of MO-LCNPs consistently 0.25 mg/mL. Data represented as mean ± standard deviation, n = 6 (3 independent experiments), two-way ANOVA * = P < 0.01. Representative orthogonal and rendered 3D laser scanning confocal microscopy z-stacks of PAO1 GFP biofilm grown in a flow cell for three days (green), treated with C. Cy5 TOB (unformulated, blue) and D. octadecyl rhodamine B chloride (R18, red)) MO-LCNPs loaded with Cy5 TOB (blue), E. Cy5 CIP (blue), F. R18 MO-LCNPs loaded with Cy5 CIP (blue). Normalized fluorescent intensities in every single z-stack of the micrograph according to time for G. Cy5 TOB unformulated, H. Cy5 TOB MO-LCNPs, I. Cy5 CIP unformulated and J. Cy5 CIP MO-LCNPs*

The difference in antimicrobial efficacy between CIP and TOB reflects their ability to penetrate biofilms. At the neutral pH of the bacterial culture media, CIP is uncharged and penetrates the biofilm matrix. The observed limited antimicrobial effect in biofilms is due to the inability to act on dormant, non-metabolically active bacteria. Due to the positive charges associated with the amino-groups, TOB is bound electrostatically to the negatively charged exopolysaccharides in the EPS of the biofilm, unable to reach the lower levels of bacteria to exert its inhibitory effect on the protein synthesis of bacteria.[9] In line with the concentration-dependent effect of TOB, higher concentrations of TOB can saturate the electrostatic interactions with the EPS, allowing TOB to penetrate the biofilm, which may explain the 1000-fold reduction from the 60 µg/mL unformulated TOB solution with the drug-free MO-LCNPs. In comparison, the TOB-loaded MO-LCNPs overcomes the electrostatic hindrance at lower concentrations.

The differences in TOB penetration were represented in confocal laser scanning fluorescence micrographs of biofilms grown with GFP-tagged PAO1 in a flow cell for three days in 1% lysogeny broth (LB) and injected with Cy5 labelled TOB as an unformulated solution or loaded into octadecyl rhodamine B chloride (R18) tagged MO-LCNPs. The unformulated fluorescently tagged antibiotic did not penetrate the biofilm, as observed in **Figure 2C**. Quantification of the fluorescence intensity in individual z-stacks through the entire biofilm demonstrated that TOB remained in the upper portion of the biofilm. The penetration did not increase over time, and TOB appeared to be immobilized throughout the experiment, with a total area under the curve of the fluorescently labelled TOB of 274, 459 and 464 AU/µm^2, for 0.5, 1 and 2 h, respectively (**Figure 2G**). When loaded into MO-LCNPs, Cy5-labelled TOB readily penetrated deep into the biofilm (**Figure 2D**). Notably, the R18-tagged MO-LCNPs did not penetrate the full thickness of the biofilm but decorated the surface of the biofilm structures, facilitating subsequent penetration of TOB. The quantified fluorescence intensities of Cy5 TOB dictated that the antibiotic was distributed across all layers of the biofilm (**Figure 2H**) with a

significantly increased area under the curve, represented by fluorescence intensities of 1209, 1509 and 1157 AU/μm^2 at 0.5, 1 and 2 h, respectively ($P < 0.01$). This is in line with Tseng *et al.*[9] who observed the inability of Cy5 TOB to penetrate the biofilm, while Cy5 dye alone penetrated.

Cy5-labelled CIP penetrated the biofilm, as observed in the unformulated solution and when loaded in the MO-LCNPs (**Figure 2E and F**). However, the penetration of unformulated CIP was not broadly distributed across the biofilm as the quantified fluorescence intensities in individual z-stacks of the biofilm reveal. CIP peaked at the surface at 0.5 h and gradually increased towards the biofilm center from 1 to 2 h (**Figure 2I**). When loaded in the MO-LCNPs, CIP distributed more evenly within the biofilm with a similar fluorescent intensity versus biofilm penetration profile to TOB MO-LCNPs (**Figure 2J**). While the area under the curves of unformulated CIP (746, 805, 1403 AU/μm^2, for 0.5, 1 and 2 h, respectively) appeared slightly lower compared to when loaded in the MO-LCNPs (1366, 1162, 1711 AU/μm^2, for 0.5, 1 and 2 h, respectively), they were not statistically different ($P = 0.15$). Besides, the areas under the curve of the unformulated and MO-LCNPs loaded (Cy5)-CIP were similar to (Cy5)-TOB loaded MO-LCNPs. Distinctly, the broad distribution of the antibiotics co-occurred with the MO-LCNPs forming a patch coating over the biofilms, subsequently improving the penetration and distribution of TOB released, similar to an adhesive patch in transdermal drug delivery, which in turn resulted in an increased antimicrobial effect.

2.3. The ability of LCNPs to enhance the antimicrobial activity of tobramycin

An extensive body of literature has demonstrated that lipid nanoparticles can enhance the effect of antimicrobials.[12] Due to the sub-micron particle size, surface and biomimetic properties, lipid nanoparticles can diffuse through many biological barriers, such as the biofilm matrix.[12, 39] However, liposomes of similar particle size did not enhance the antimicrobial activity of

TOB against MBEC® grown PAO1 biofilms (at an equivalent concentration of 15 µg/mL) (**Figure 3A**), suggesting the advanced activity against *P. aeruginosa* biofilm was unique to the LCNPs. Liposomal carriers have been widely explored to enhance the antimicrobial activity of antibiotics, particularly aminoglycosides, due to their fusogenic and surface properties.[14, 40] Liposomes with lower rigidities and transition temperatures (termed Fluidsomes™) were more favorable *in vivo* to increase the antimicrobial activity of aminoglycosides. Eradication of *P. aeruginosa* respiratory infection in Sprague-Dawley rats was correlated with the fusion of liposomes with the bacteria and subsequent increased antibiotic concentrations in the interstitial space.[14, 40] Liposomes are a simplified version of LCNPs. Various phospholipid based liposomes have been proposed and are patented as formulations to increase the activity of TOB, gentamicin and amikacin.[14, 40-43] Recently, there has also been the successful marketing of Arikayce®.[15]

While liposomes do have the potential to increase the effectiveness of antibiotics, certain phospholipid combinations are required to achieve this. We have observed that in comparison to liposomes composed of 1, 2-distearoyl-sn-glycero-3-phosphocholine (DSPC) and 1, 2-dipalmitoylphosphatidylglycerol (DPPG), both MO- and PHY- LCNPs significantly enhanced the antimicrobial effect of TOB. The soft, 3-D crystalline structures of lipids bilayers in LCNPs have also demonstrated fusogenic properties with biological lipid bilayers (i.e. cell membranes) due to the similarity in composition.[44, 45] Unlike unilamellar liposomes, the bilayers in LCNP with infinite minimal surfaces, provide a greater surface area for interaction with cells.[46] LCNPs have shown superior skin retention compared to liposomes,[47] suggesting the multi-faceted lipid bilayer and a higher degree of localized curvature enhanced the penetration and interaction with the biological components compared to unilamellar vesicles.

Interestingly, even though they have different chemical properties, both MO-LCNPs and PHY-LCNPs demonstrated similar 1000-fold reductions in antimicrobial activity at 15 µg/mL TOB against the simplified PAO1 biofilms (compared to unformulated TOB) (**Figure 3A**). Although PHY has known antimicrobial properties,[48] at the concentration used, no innate activity was observed. Decreasing the concentration of MO-LCNPs five-fold (to 0.05 mg/mL), while maintaining the TOB concentration at 15 µg/mL did not alter the enhanced anti-biofilm effect from loading TOB into the LCNPs. The similarities in the liquid crystalline structure of MO- and PHY-LCNPs may facilitate the interaction with the biofilm matrix and the formation of the patch that drives the enhanced effect of TOB.

Consequently, the R18 labelled MO-LCNPs demonstrated an enhanced fusion efficiency with PAO1 planktonic bacteria in a lipid-mixing assay compared to the unformulated solution of the dye (**Figure 3C**). The significant fusion potential of TOB loaded MO-LCNP coincided with a decreased minimum inhibitory concentration (MIC) compared to the unformulated solution in planktonic PAO1 (**Figure 3C**), which further suggests the LCNPs may increase the bacterial bioavailability of the aminoglycoside antibiotic. While the liposomes did not fuse with *P. aeruginosa* (data not shown), the LCNPs fusion may have secondary facilitated the enhanced antimicrobial effect and the patch formation around the biofilm.

While the nanoparticle diameter was similar between the LCNPs and liposomes, the surface zeta potential differed, where the LCNPs zeta potential increased towards -9.5 and -13.4 mV (for MO and PHY, respectively), and the liposomes were negatively charged (-43.5 mV). Messiaen *et al.* [49] demonstrated that negatively charged nanoparticles were immobilized near the biofilm cell clusters but failed to modulate the antimicrobial activity due to repulsion from the negatively charged cell walls of bacteria. The enhanced fusion efficiency of the LCNPs with *P. aeruginosa* suggests the LCNPs are not repelling from the bacteria cell, but adhering to the

biofilm matrix as a patch coating (**Figure 2D**), leading to a steeper concentration gradient and thus enhancing penetration of TOB through the biofilm matrix. While the slightly negative surface charge of LCNPs would be subjected to some repulsive forces from the biofilm matrix, the slight biofilm penetration of LCNP appeared enough to release TOB directly to the bacteria residing within the biofilm matrix, increasing the total concentration inside the biofilm. Similarly, slightly negative or near-neutral surface charged nanoparticles improved the targeting of the biofilm compared to highly negative or positive particles.[39, 50]

The enhanced antimicrobial effect of TOB MO-LCNPs did not differ between the two *in vitro* biofilm models used in the present study (i.e. the MBEC® model and a simple (well-plate) biofilm model). Compared to a 100-fold-reduction after TOB solution treatment, a 10'000-fold-reduction in PAO1 load resulted from TOB MO-LCNPs treatment at 15 µg/mL TOB (in 0.05 mg/mL MO-LCNPs), using the simple biofilm model (**Figure 3A**). Compared to the simple biofilm model, where the biofilm rests on the bottom of a well plate, the biofilm on the polystyrene pegs in MBEC® model is suspended and reduces the bias of potentially increased (nano)particle settlement.[51] The simple biofilm may also have structural and metabolic differences to the MBEC® biofilm model; however, it was out of the scope of the present study to compare the structural and metabolic differences between the models. The scanning electron micrograph of the MBEC® biofilm visually appears more robust than the simple well-plate biofilm imaged by laser scanning confocal microscopy (**Figure 3C and D**, respectively). Regardless of the *in vitro* biofilm model employed, the antimicrobial effect of TOB was increased by loading into LCNPs.

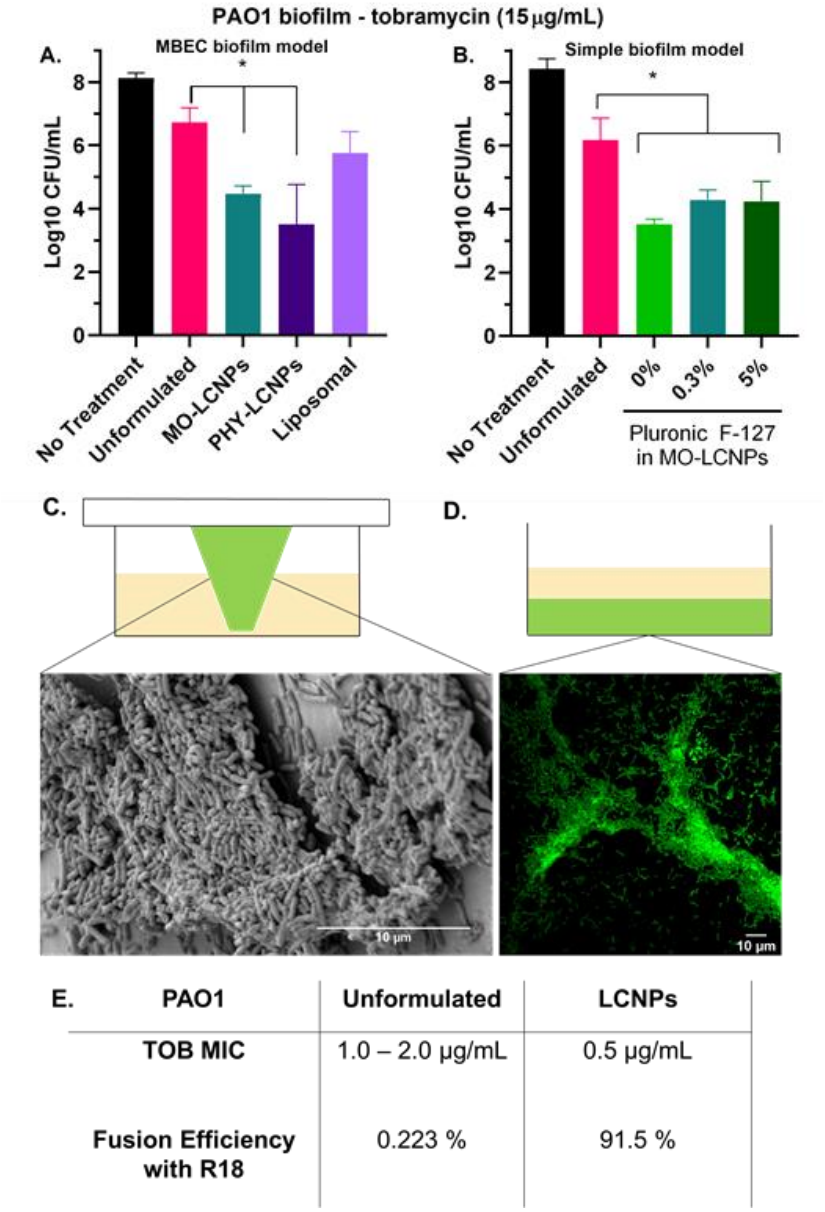

E. PAO1	Unformulated	LCNPs
TOB MIC	1.0 – 2.0 µg/mL	0.5 µg/mL
Fusion Efficiency with R18	0.223 %	91.5 %

Figure 3. *The antimicrobial activity of tobramycin (TOB) in different formulations and biofilm models. A. The total amount of PAO1 remaining from the MBEC® model after treatment with tobramycin (15 µg/mL) as an unformulated solution (pink) and formulated as MO-LCNPs (teal), PHY-LCNPs (dark purple) and DSPC: DPPG liposomes (light purple). B. The total amount of PAO1 remaining from the simple (well-plate) biofilm method after treatment with tobramycin (15 µg/mL) as an unformulated solution (pink) or formulated in MO-LCNPs (teal) and MO-LNCPs containing no (dark green) or a higher amount of Pluronic F127 (light green). MO-LCNPs = 0.05 mg/mL. Data represented as mean ± standard deviation, n = 9 (3 independent experiments), one-way ANOVA * P < 0.01. C. Representative scanning electron microscopy image of PAO1 biofilm grown on MBEC® model compared to D. representative laser scanning confocal microscopy image of GFP-PAO1 biofilm grown in simple biofilm model and D. Minimum inhibitory (MIC) concentrations of tobramycin (TOB) and fusion efficiency of R18 with PAO1 planktonic bacteria as an unformulated solution or loaded in MO-LCNPs, n = 8 (2 independent replicates).*

The surface functionalization can dictate the permeation of a particle through a biological barrier, with extensive work focused on mucus penetrative PEGylated nanoparticles.[52, 53] It has been shown that nanoparticles coated with a sufficient amount of low molecular weight polyethylene glycol (PEG) enhanced the particle penetration through mucus, regardless of the nature of the particle core.[53-55] Pluronic® F-127, a triblock copolymer of PEG-PPO-PEG, has demonstrated drastically enhanced mucus penetration *in vitro*, *ex vivo* and *in vivo* when used as a coating of sub- 300 nm organic, polymeric and lipid nanoparticles.[52, 53] While the biofilm matrix has a different composition to mucus, which is typically rich in mucin, both create a biologically physical barrier. [56, 57] Consequently, we hypothesized that modulation of the density of Pluronic® F-127 coating might also affect biofilm penetration of LCNPs, and consequently, affect antimicrobial efficacy.

Interestingly this was not observed. Fabrication of LCNP devoid of Pluronic® F-127 and LCNP prepared with 5% w/v did not alter the anti-biofilm effect of MO-LCNPs (**Figure 3A**). The particle size of the 'original' MO-LCNPs fabricated with 0.3% (w/v) Pluronic® F-127 was approximately 164 nm. The increase of the polymer, did, however, significantly reduce the particle size of the LCNPs to approximately 85 nm while only a modest change on particle size was observed for LCNPs containing no Pluronic® F-127 (**Figure 1a**). As shown in **Figure 3B** and compared to unformulated TOB solution, TOB MO-LNCPs further reduced the bacterial load by 100-fold, regardless of the polymer concentration and particle size, suggesting benefits of the liquid crystalline structure of LCNPs to impart antimicrobial activity. While exploring the mucus-penetrative properties of the LCNPs was out of the scope of the present study, the advanced effect of the TOB LCNPs formulations with and without Pluronic® F-127 coatings and compared to other nanoparticles (i.e. liposomes) suggests the liquid crystalline structure specifically facilitates the enhanced activity of TOB.

2.4. LCNPs increase tobramycin penetration across the biofilm matrix but not the epithelium barrier

In the CF bronchial epithelium cell line (CFBE41o-), the MO-LCNPs were considered non-toxic (viability > 85%) at a concentration range from 0.01 – 0.25 mg/mL of MO, while the PHY-LCNPs were non-toxic below 0.01 mg/mL (Supplementary material, Figure 1). While both MO and PHY are generally recognized as safe (GRAS) compounds by the Food and Drug Administration (FDA) and are used widely in the cosmetic and pharmaceutical industry, the cellular toxicity profiles were consistent with previous reports.[19] The higher toxicity of PHY-LCNPs is also related to their greater potential to fuse with cell membranes compared to MO-LCNPs, with a greater propensity to cause hemolysis in healthy cells.[44, 58] Given the higher toxicity of PHY-LCNPs and the instabilities of the formulation, all proceeding studies focused on MO-LCNPs.

As a small hydrophilic molecule, the transport of TOB across a cell monolayer is likely to occur via the paracellular route, which is restricted by tight intercellular junctions.[59, 60] Correspondingly, the apparent permeability coefficient (P_{app}) of (unformulated) TOB was 8.1 x 10^{-7} $cm.s^{-1}$ (**Figure 4A**) and comparable to the P_{app} of sodium fluorescein, an established paracellular transport marker (6.8 x 10^{-7} $cm.s^{-1}$, **Figure 4B**). Incubation with EDTA, a known tight junction disrupter, led to the marked increase in sodium fluorescein P_{app} (5.0 x 10^{-5} $cm.s^{-1}$), providing further evidence for the paracellular pathway. As demonstrated in **Figure 4A** and **B**, the LCNPs did not alter the permeability of TOB or sodium fluorescein across tight CFBE41o- epithelial cell monolayers, with a P_{app} of 1.2 x 10^{-6} $cm.s^{-1}$ and 1.4 x 10^{-6} $cm.s^{-1}$, respectively ($P > 0.05$). As PEGylated lipid-based particles, the hydrophobicity may increase (trans)cellular uptake and transport of the LCNPs and loaded compounds. Compared to the high P_{app} of the lipophilic dye (R18, 4.0 x 10^{-6} $cm.s^{-1}$), the P_{app} of the lipophilic fluorescent dye

decreased to 2.4 x 10^{-7} cm.s^{-1}, following loading in the MO-LCNPs, indicating limited transcellular transport of the LCNPs across the CFBE41o- monolayer (**Figure 4C**).

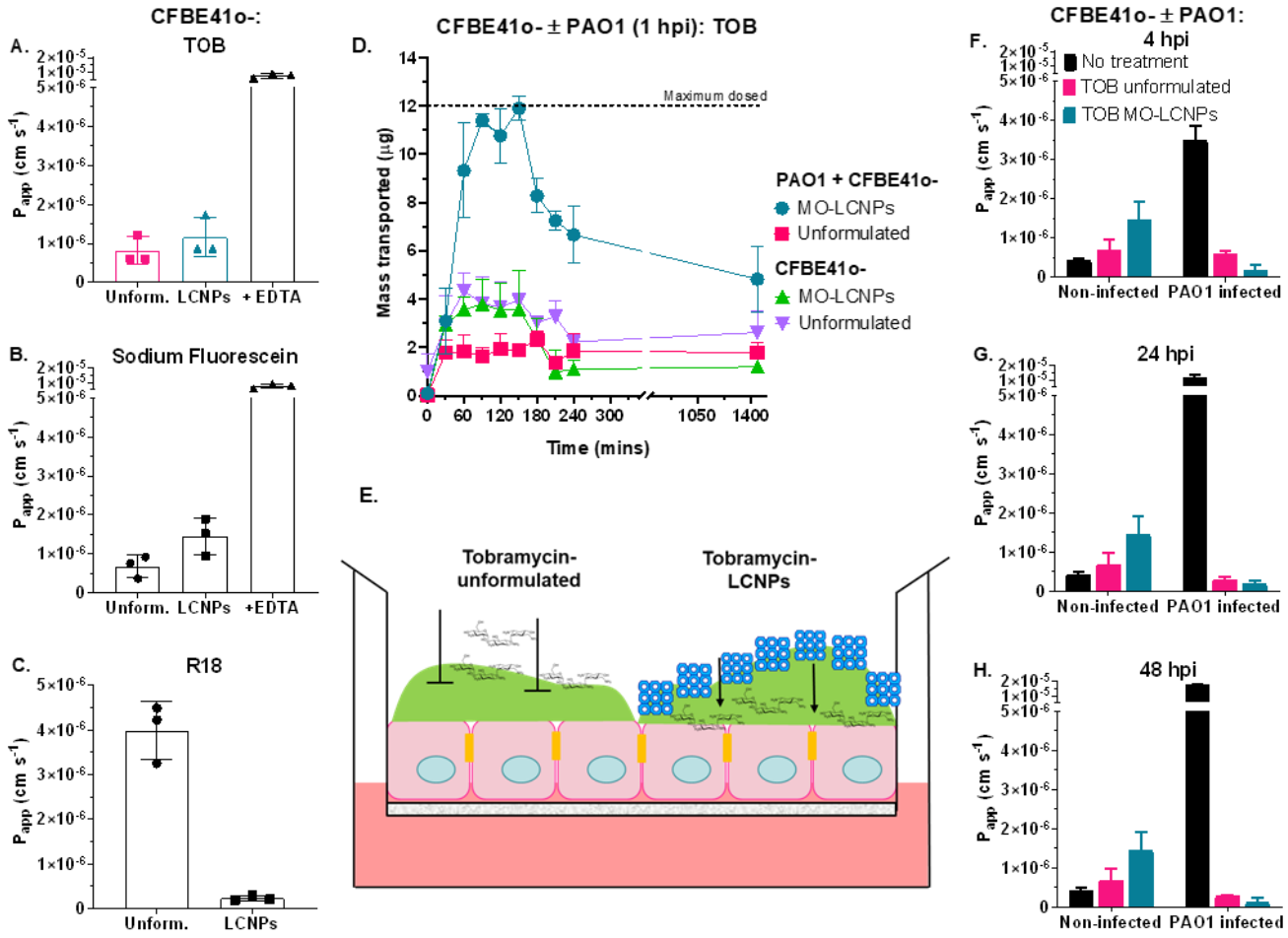

Figure 4. *Tobramycin (TOB) LCNPs penetrate PAO1 biofilm but not healthy CFBE41o- epithelium. The apparent permeability coefficient indicating; A. TOB, B. sodium fluorescein and C. Octadecyl Rhodamine B chloride (R18) transport as an unformulated solution or loaded in MO-LCNPs across CFBE41o- cells (0.05 x 10^6 cells/well in 12-well Transwells® inserts), TEER 448 Ω*cm^2, p. 4.86, (MO-LCNPs concentration 0.05 mg/mL). D. TOB mass transport across CFBE41o- (p 4.87, 4.88,) 0.05 x 10^6 cells/well seeded on Transwell® inserts with and without PAO1 biofilm infection, following nebulized treatment with 12 µg of unformulated tobramycin or 12 µg of MO-LCNPs (MO = 0.025 mg/mL) using the Aerogen® Pro (vibrating mesh nebulizer) and deposition device. E. A schematic representing the difference in the transport of tobramycin across the biofilm and epithelium layer. F.-H. The apparent permeability coefficient of sodium fluorescein across healthy and PAO1 infected CFBE41o- cells (0.05 x 10^6 cells/well in 12-well Transwells® inserts, p. 12-15, after F. 4 h post-infection (hpi), G. 24 hpi and H. 48 hpi, ± TOB (12 µg) nebulized as an unformulated solution or loaded in the MO-LCNPs. Data represented as mean ± standard deviation, n = 5 (2 independent experiments).*

Limited penetration across the epithelium monolayer suggests limited systemic absorption and bioavailability of TOB following aerosolization into the lungs. Previously, in CF patients, aerosolized TOB resulted in limited systemic absorption and a low bioavailability of 9.13%.[61] The local administration of TOB to pulmonary tissue is highly valuable to the concentration-dependent effect of aminoglycosides, whereby obtaining sufficient concentrations in the pulmonary tissue is critical to antimicrobial activities, rather than maintaining the concentration for an extended period.[62] Since the LCNPs did not further enhance the permeability of TOB across the bronchial epithelium, systemic exposure to TOB should be limited when delivered by inhalation of an aerosolized MO-LCNPs formulation. Besides maximizing the antimicrobial effect, local pulmonary administration reduces off-target adverse effects of aminoglycosides, including nephro-, oto- and neuro-toxicity.[63]

Accurate and reliable *in vivo* models of lungs infected with *P. aeruginosa* biofilms to evaluate antimicrobial therapy are severely lacking.[26] A sophisticated, biologically-relevant *in vitro* model based on human bronchial epithelial cells (CFBE41o-) infected with mature, three-day-old *P. aeruginosa* biofilms at the air-liquid interface, [Horstmann *et al*., manuscript in preparation], permits biological relevant quantification of the bacterial and human host response to TOB MO-LCNPs treatment compared to the unformulated antibiotic. This model mimics a chronic lung infection in the bronchial region and is particularly relevant for pulmonary infections observed in CF patients, as the used CFBE41o- cell line also contains the CFTR mutation.[64]

The transport of TOB across the biofilm and human bronchial epithelial cells was quantified immediately after nebulization either as a solution or after encapsulation in the MO-LCNP nanocarriers. While the solution and MO-LCNPs demonstrated limited transport of TOB across healthy CFBE41o- cell monolayers, immediately upon *P. aeruginosa* biofilm infection, the

tight junctions and barrier function of CFBE41o- is jeopardized and becomes leaky. In corroboration with the visual representation of TOB in biofilms (**Figure 2C and D**) on top of the epithelial cell monolayer, TOB transport was significantly higher in the MO-LCNPs than the unformulated solution. At the peak of 2.5 h after nebulization, 99.2% of TOB reached the basolateral compartment, compared to 15.8% of the unformulated TOB (**Figure 4D**). The MO-LCNPs formulation increased the area under the curve 3.5-fold, similar to the laser scanning confocal micrographs quantified in **Figure 2D**. Invariably, the LCNPs transported more TOB through the biofilm than the unformulated antibiotic. By assessing the sequential barrier integrity via sodium fluorescein transport, after 4 h post-infection, the barrier integrity of the CFBE41o- was found equivalent to the healthy cell monolayer following treatment with TOB either as an unformulated solution or in the MO-LCNPs (**Figure 4F**). In comparison, without antibiotic treatment, the barrier diminished 4 h post-infection, indicative by the rising P_{app} (P_{app} 3.5 x 10^{-6} $cm.s^{-1}$, **Figure 4F**) and was non-existent beyond 24 h post-infection (**Figure 4G**), where limited cells remained.

In sequence with previous work, the tight junctions were compromised and explain the initially increased transport of TOB {Horstmann *et al.*, manuscript in preparation). Upon clearance of the infection, the epithelial barrier function re-established, as observed in **Figure 4F-H**. Considering the single-cell monolayer in the present study lacks additional biological support, upon incomplete bacterial killing, the barrier function of the cells requires time to recover, further resulting in the increased transport of TOB at the early stages of infection. However, without a full animal model, it is not known if MO-LCNPs TOB would increase the systemic absorption through penetration of the epithelial barrier.

2.5. Nebulized tobramycin LCNPs eradicates a chronic *P. aeruginosa* biofilm infection on the lung epithelium

Consistent with previous findings in a simple *in vitro* biofilm model and in corroboration with the enhanced penetration of TOB from the MO-LCNPs across the biofilm, at 24 h, after a single 12 µg nebulized dose to the chronic infection model, the antimicrobial effect of TOB was 100-fold higher compared to the unformulated antibiotic. The three-day-old biofilm, containing 4 x 10^8 CFU/mL of *P. aeruginosa*, was reduced to 7.4 x 10^3 CFU/mL at 24 h after nebulization with unformulated TOB and 8.5 x 10^1 CFU/mL after nebulization of the MO-LCNPs TOB (Supplementary Material, Figure 2). The confocal microscopy images in **Figure 6** depict the biofilms infecting the bronchial epithelial cells at 4 h as small 'micro-colonies' compared to the dense biofilms observed in the flow cell and MBEC® models, represented in **Figure 2C-F** and **Figure 3C**, respectively. Comparatively, these 'micro-colonies' of biofilms in the co-culture cell model are more realistic to the suspected *in vivo* biofilm, as previously described by Bjarnsholt *et al.*[30]

Following 48 h post-infection, the effect of TOB MO-LCNPs increased further and did not statistically differ between one or two doses in the 48 h period, leaving 2 CFU/mL or 0 CFU/mL and practically eradicated the *P. aeruginosa* biofilms from the epithelium (**Figure 5A**). The single and dual dose of TOB MO-LCNPs were more effective at 48 h compared to 24 h. In comparison, after one and two nebulized doses of the unformulated TOB within 48 h, 1.2 x 10^3 CFU/mL and 5.4 x10^1 CFU/mL of *P. aeruginosa* remained, respectively. Without removing the single dose of the unformulated TOB, the effect did not differ between 24 h and 48 h. Comparatively, while removing the treatment and replacing it with a second dose increased the effect, it still did not eradicate the infection. Importantly, the significantly enhanced antimicrobial effect from TOB MO-LCNPs was not accompanied with a decrease in the cell viability of the epithelium monolayer, as demonstrated by consistent cell viabilities above 80%, observed via LDH assay (**Figure 5B**), bright-field light microscopy and in the laser scanning confocal micrographs in **Figure 6G-I**. The MO-LCNPs visibly attracted to the GFP-tagged *P.*

aeruginosa biofilm as observed in the confocal micrographs (**Figure 6H**), which resulted in the higher dose of TOB transported across the biofilm compared to the unformulated antibiotic, leading to the advanced eradication of the infection immediately after two doses (i.e. 48 h post-infection (hpi), **Figure 6I).**

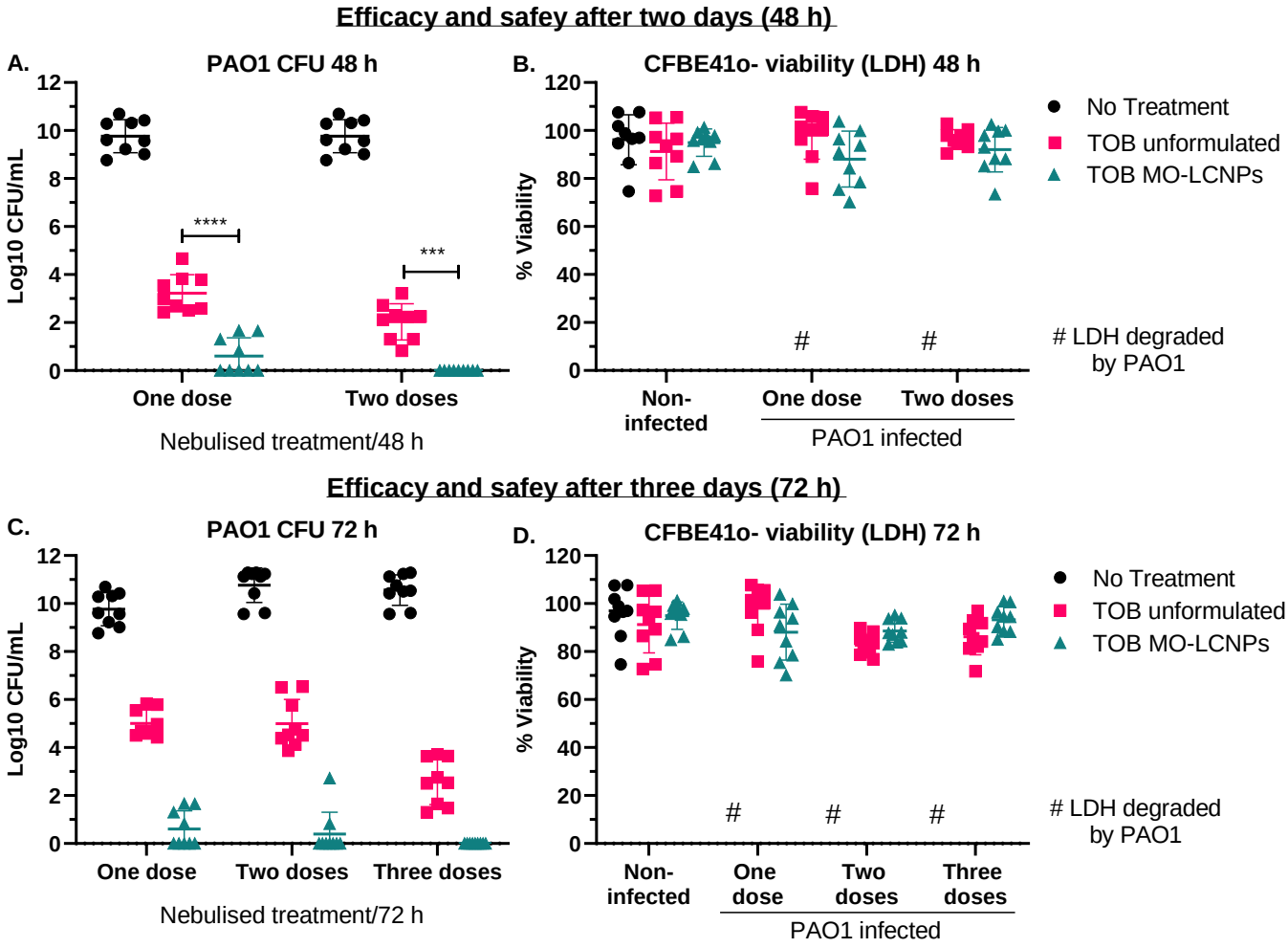

Figure 5*. Tobramycin liquid crystal nanoparticles (TOB LCNPs) eradicate PAO1 biofilm from CFBE41o- chronic infection model. The efficacy and viability of 12 µg tobramycin as an unformulated solution (pink squares) or loaded in MO-LCNPs (teal triangles) in CFBE41o- monolayer (p 4.83-7, and p 12-18, 0.05 x 10^6 cells/well) infected with PAO1 biofilm, following 48 h or 72 h after nebulized treatment using the Aerogen® Pro (vibrating mesh nebulizer) and deposition device. A. total amount of PAO1 remaining after one or two treatments per 48 h, B. CFBE41o- viability assessed via LDH assay compared to cells treated with 5% Triton X. C. total amount of PAO1 remaining after one, two or three treatments per 72 h, and B. CFBE41o- viability assessed via LDH assay compared to cells treated with 5% Triton X. Data represented as mean ± standard deviation, n = 9 (3 independent experiments), two-way ANOVA with Tukey multiple comparison test **** = P < 0.0001*

Following 72 hpi, the advanced antimicrobial effect of TOB MO-LCNPs did not statistically differ between one, two or three doses, leaving 4 CFU/mL, 2 CFU/mL and zero CFU/mL (P = 0.99, 0.76, 0.97), respectively and thus eradicating the *P. aeruginosa* biofilms from the epithelium (**Figure 5A).** In comparison, after one, two and three nebulized doses of the unformulated TOB within 72 h, 9.8 x 10^4 CFU/mL, 1.7 x 10^5 CFU/mL and 2.7 x10^2 CFU/mL of *P. aeruginosa* remained, respectively. Similar to 48 hpi, one or two doses of unformulated TOB resulted in an equivalent increased PAO1 load, while a third dose increased the antimicrobial effect, it still did not eradicate the PAO1 infection. Both the unformulated TOB and TOB MO-LCNPs maintained the epithelium cell monolayer viability after 72 h and did not adversely affect the epithelial cells (**Figure 5D** and **Figure 6L**). Together, the enhanced action of TOB MO-LCNPs against *P. aeruginosa* biofilms in such an infected human pulmonary cell culture model confirmed the previous *in vitro* data from biofilm-only models.

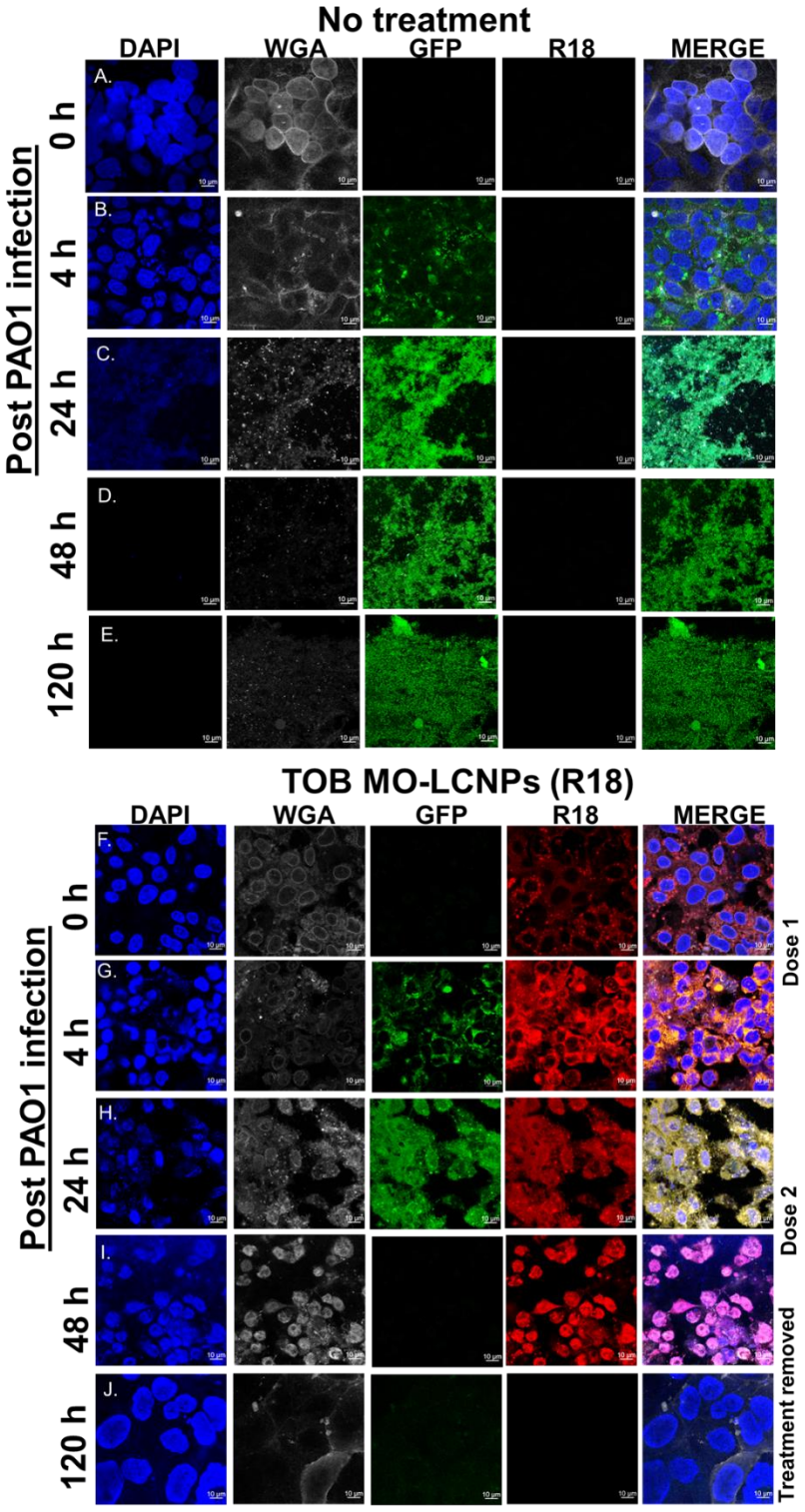

Figure 6. Representative splits and merged laser scanning confocal microscopy images of chronic infection model. CFBE41o- cells (nuclei stained with DAPI, WGA Alexa Fluoro 633 stained membranes) infected with PAO1 (GFP-tagged) with no treatment (A.-E.) compared to TOB MO-LCNPs (tagged with Octadecyl Rhodamine B chloride, R18) nebulized treatments (F.-J.) The TOB MO-LCNPs were then removed via refreshing the basolateral medium at 48 h post-infection, and the cells were kept for an extra 72 h.

The eradication following either two or three doses of TOB MO-LCNPs is very promising. In previous infected co-cultures models of CFBE41o-, despite an undetectable amount of bacteria via CFUs, bacteria were observed via confocal microscopy.[28] Similarly, in some samples, small colonies of bacteria were detected after a second dose of TOB MO-LCNPs via confocal microscopy, despite a zero bacterial cell count (in CFU/mL). While initially sensitive to antimicrobial treatment, the residual *P. aeruginosa* colonies isolated from CF patients frequently demonstrate high levels of persistence.[65] The persister colonies contribute to the recalcitrance of CF lung infection and have been attributed to the dormancy and low metabolic activity of bacteria rather than genetic changes.[66, 67] Once the antibiotic is removed, or the culture is incubated longer, the persister cells may switch to higher metabolic states and resume growth, continuing the cycle of infection.[68]

To examine if any dormant colonies could re-populate, the basolateral cell media was refreshed 24 h after the second and third dose, and the samples were kept for another two days. Following clearance of the second dose of the TOB MO-LCNPs (via refreshing the cell media), the CFBE41o- cell monolayer remained relatively bacterial free (on average) for at least two more days (**Figure 7B**), and the cell viability was maintained (**Figure 7C**), as further observed in the confocal micrograph in **Figure 6J**. A similar trend was observed following the third dose of TOB MO-LCNPs (**Figure 7C** and **D**), indicating it was equivalent to the dual dose regimen. However, two-to-three samples out of nine replicates demonstrated *P. aeruginosa* re-growth, shifting the mean PAO1 load to 2.9×10^1 CFU/mL and 1.9×10^1 CFU/mL at 72 h post two and three doses, respectively. The inability of the unformulated TOB to eradicate the biofilm infection led to an exponential increase in *P. aeruginosa* after removal of both the second and third dose, where the infection was comparable to the no treatment control at 72 h post-dose (**Figure 7A** and **C**), and destroyed the CFBE41o- cell monolayer (Supplementary Material, Figure 3).

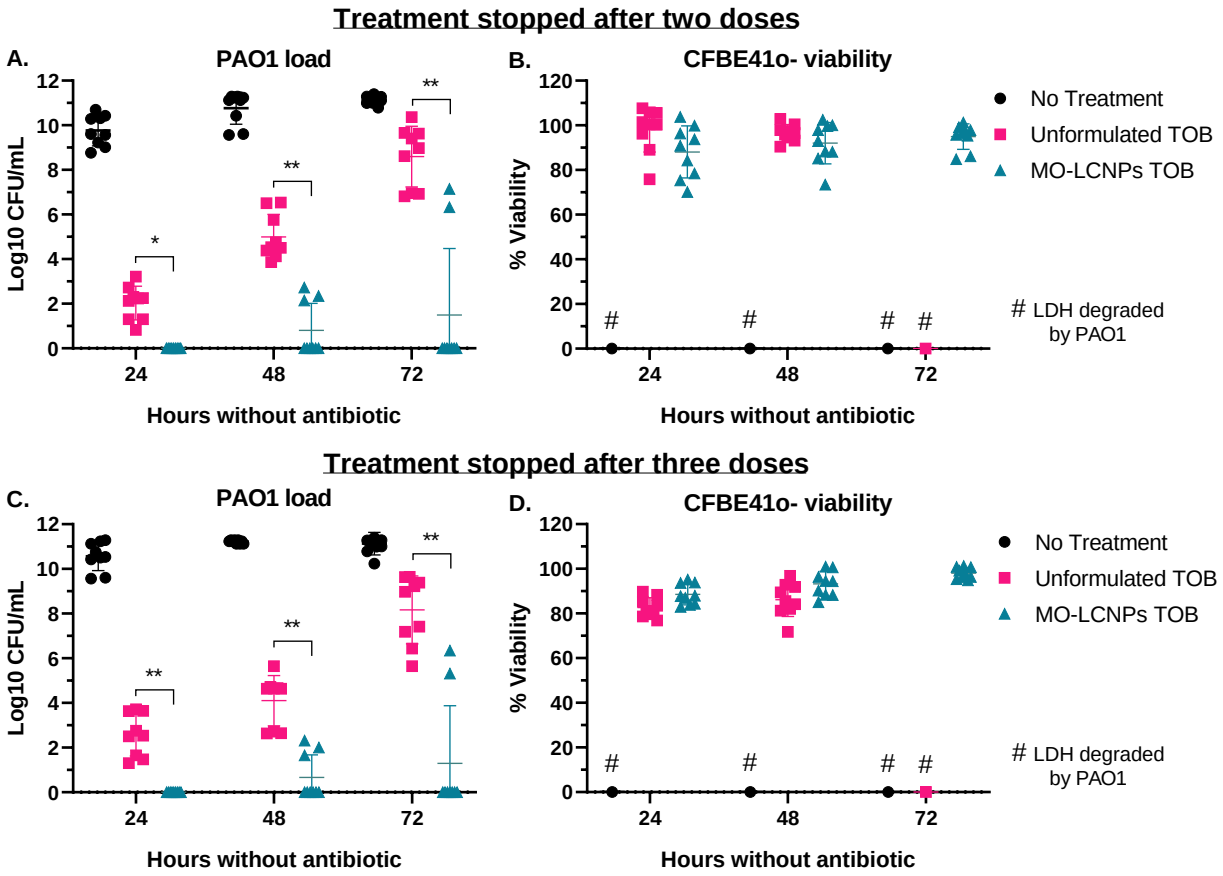

Figure 7. *The reversibility of PAO1 after treatments were removed from CFBE41o- (p 12-18, 0.15 x 10^6 cells/well infected with PAO1 biofilms). The cells were previously treated with either 12 µg TOB unformulated (pink squares) or TOB MO-LCNPs (teal triangles, MO = 0.025 mg/mL) at 24 h intervals via nebulization using the Aerogen® Pro (vibrating mesh nebulizer) and deposition device. After either two-doses or three-doses, the basolateral media was replaced, washing away the treatments, and samples were kept for up to 72 h (without antibiotic). A. The total amount of PAO1 remaining after two-doses and B. CFBE41o- viability, C. total amount of PAO1 remaining after three doses and B. CFBE41o- viability. Data represented as mean ± standard deviation, n = 9 (3 independent experiments), two-way ANOVA with Tukey multiple comparison test * = P < 0.01, ** = P < 0.001*

The time taken for an organism to re-grow following exposure to TOB, known as the post-antibiotic effect, depends on the exact concentration and clearance of the antibiotic. In line with the present data, the predicted interval is 24 h and permits once-daily dosing regimens to reduce the side effects of TOB.[69] In early cystic fibrosis lung infections with *P. aeruginosa*, TOB is given for 28 days, and 66% of patients remain infection-free 27 months in early-years of infections.[70] Although for late-stage, mucoid *P. aeruginosa* infections, where biofilms are

predominant, eradication is not possible.[5] Besides, the presence of persister cells is often unrecognized. It was out of the scope of the present study to further examine the metabolic and genetic basis of the colonies growing after treatment was removed. As observed, additional doses or higher concentrations of TOB will not affect dormant bacteria. Previously, chemical switches have been used to change the metabolic state of the persister cells, increasing their sensitivity to antibiotics.[71] Regardless, the model used here demonstrated the possible eradication of *P. aeruginosa* (mucoid) biofilms from the bronchial epithelial cells after two to three doses of TOB MO-LCNPs.

Notwithstanding the issue of re-populating dormant cells, we have demonstrated an avenue to overcome the significant EPS matrix barrier that precludes the antimicrobial effect of TOB. In contrast to the advanced effect of TOB MO-LCNPs, such eradication was never achieved with the unformulated TOB in this rapid time frame. Future studies will further investigate the effects of TOB MO-LCNPs in pre-clinical studies and examine intermittent therapy to achieve life-long *P. aeruginosa* infection eradication.

3. Conclusion

LCNPs advance the antimicrobial activity of TOB through enhanced penetration across *P. aeruginosa* biofilm in simple *in vitro* models and sophisticated infected co-cultures of bronchial epithelial cell monolayers. Together, the lipid liquid crystalline structure, sub-micron particle size, and neutral surface charge aid the enhanced penetration of TOB across the biofilm barrier, while the LCNPs can also fuse with single *P. aeruginosa* cells, permitting advanced antimicrobial effects. Unlike CIP MO-LCNPs, delivery of TOB MO-LCNPs resulted in a 100-fold enhanced antimicrobial activity compared to an unformulated TOB solution. Drug-free LCNPs did not show an antimicrobial effect, and TOB loading in the LCNPs was critical to the

enhanced effect. The performance of LCNPs could not be replicated with liposomal formulations of TOB and was robust against surface stabilizer concentrations. In an advanced *in vitro* model of human pulmonary epithelial cells grown as a monolayer on permeable filter supports at an air-liquid interface and infected with pre-grown *P. aeruginosa* biofilms, the TOB MO-LCNPs eradicated the infection after two days. The LCNPs could be nebulized, without affecting the particle size and successfully carry TOB to the bacterial biofilm without increasing the permeability across the epithelium, suggesting that they are suitable as an advanced, local pulmonary inhalation therapy.

4. Experimental Section/Methods

4.1. Formulation development and characterization

4.1.1. Liquid crystal nanoparticles (LCNPs)

Liquid crystal nanoparticles (LCNPs) were formed with monoolein (MO, Myverol 18-99K (part number: 5D01253, Kerry Ingredients and Flavours Egham, Surrey, UK) or phytantriol (PHY, DSM Heerlen, the Netherlands), via the hydrotrope dilution method.[25] MO or PHY (100 mg), Pluronic® F-127 (15 mg, Sigma-Aldrich, Castle Hill, NSW, Australia) and propylene glycol (0.26 g, Sigma-Aldrich, Castle Hill, NSW, Australia) were mixed by vortexing for 2 minutes and then completely dissolved in 10 mL chloroform (HPLC grade, 1% ethanol, ChemSupply, Port Adelaide, SA, Australia) in glass scintillation vials. A stream of nitrogen gas evaporated the chloroform, leaving behind a thick lipid film on the inside wall of the flask. After that, 0.1 mL of tobramycin (up to 300 mg/mL) (TOB, free base, ChemSupply, Port Adelaide, SA, Australia) or ciprofloxacin (up to 60 mg/mL) (CIP hydrochloride, Sigma-Aldrich, St. Louis, MO, USA) in 0.9% NaCl, was added to hydrate the lipid-hydrotrope mixture and vortex-mixed for 30 seconds. The hydrated lipid-hydrotrope mixture was then further diluted

to 5 mL with purified (MilliQ) water and vortex-mixed until a homogenous white emulsion formed (2 minutes).

The amount of Pluronic® F-127 in the MO-LCNPs TOB formulation was also varied to determine the effect the surface stabilizer had on the antimicrobial effect. The original formulation had 0.3% w/v in the final preparation, where MO-LCNPs were also prepared without any Pluronic® F127 and a higher amount (5% w/v). Both no Pluronic® F-127 MO-LCNPs TOB and 5% w/v Pluronic® F-127 MO-LCNPs TOB were included as the treatments, at a dose of 15 µg/mL TOB, 0.025 mg/mL MO-LCNPs.

4.1.2. Liposomes

Liposomes were prepared from a 1:1 mixture of 1, 2-distearoyl-sn-glycero-3-phosphocholine (DSPC) and 1, 2-dipalmitoylphosphatidylglycerol (DPPG) (0.05/0.05 % w/w, Sigma-Aldrich, St. Louis, MO, USA) dissolved in methanol (HPLC grade, ChemSupply, Port Adelaide, SA, Australia). Using a Nanoassemblr® (Precision Nanosystems, Vancouver, BC, Canada), the benchtop microfluidic device mixed a 1.5:1 (aqueous: organic) ratio of TOB in solution (Tris-NaCl, 50 – 150 mM) and DSPC/DPPG in methanol with a total flow rate of 12 mL/min. The collected liposomes were then stirred overnight to evaporate any residual methanol in the mixture.

4.1.3. Particle size and zeta potential

Diluted samples of LCNPs and liposomes (1:1000) in water (viscosity 0.887 cP) were analyzed using dynamic light scattering and phase analysis scattering at 25^{o}C using the using a Zetasizer Nano ZS (Malvern, Worcestershire, UK) to determine the particle size and zeta potential, respectively. The built-in software-enabled determination of the mean hydrodynamic diameter (reported as the z-average) and the particle size distribution (reported as the polydispersity index, PDI) over 15 triplicate measurements, with unimodal distributions.

4.1.4. Drug load and release

As previously described, pressure ultrafiltration stirred cell (Amicon®, Merck Millipore, Bayswater, VIC, Australia) indirectly determines the total amount of TOB loaded in the LCNPs and liposomes.[25] 2.5 mL of the LCNPs suspensions (undiluted) was transferred into the cell containing a pre-soaked ultrafiltration disc made of biomax polyethersulfone, 500 kDa NMWL (Merck Millipore, Bayswater, VIC, Australia). Upon applying 100 kPa of nitrogen gas, the LCNPs were subjected to ultrafiltration that produces a filtrate that is free of the LCNPs due to the particle size restriction of the ultrafiltration disc. The filtrate was quantified to verify the unloaded antibiotic portion, while the total amount of TOB loaded was determined through dissolving the concentrated LCNPs with 5% v/v Triton X (Sigma-Aldrich, St. Louis, MO, USA).

The loaded LCNPs formulations were diluted 1:5 with buffered media (0.01 M Phosphate Buffered Saline (PBS) buffer, pH 7.4) in the pressure ultrafiltration cell to determine the release. The mixture was magnetically stirred and at specific time points (0, 5, 10, 15, 30, 45, 60, 90, 120, and 240 mins) 0.5 mL samples were collected by applying 100 kPa of nitrogen gas. Immediately after each sample was removed, it was replaced with 0.5 mL of fresh PBS.

TOB concentrations were quantified by high-performance liquid chromatography (HPLC) with UV detection (Shimadzu, Kyoto, Japan), following a derivatization procedure. The derivatization of TOB standards and release samples was performed with 1, 2-dinitrofluorobenzene (DNFB) (15 mg/mL in 100% ethanol), as previously described by Russ *et al.* [72] and the TOB USP monograph. Briefly, individual TOB solutions (80 µL) in 50 mM Tris buffer (pH 7.4) were doped with 10 mM sulphuric acid, 200 µL of 15 mg/mL DNFB and 200 µL of 25 mM Tris in 80% dimethyl sulfoxide (DMSO) in a glass vial. The vials were then placed in a 70°C water bath for 20 minutes to allow the derivatization reaction to proceed. After 20 minutes, the vials were cooled to room temperature and diluted with acetonitrile (520 µL) for HPLC analysis.

Sample separation was carried out on a Phenomenex Luna 5 µm C18 100 Å (250 x 4.6 mm) (Torrance, USA) column equipped with a column guard. The system was maintained at 40°C, with an injection volume of 20 µL and elution with a mobile phase at a flow rate of 1.2 mL/min. The mobile phase was a mixture of 45% (V/V) of 17 mM Tris and 20 mM sulphuric acid in water and 55% (V/V) of acetonitrile (ChemSupply, Port Adelaide, SA, Australia). Each sample was analyzed over 11 minutes at a detection wavelength of 365 nm, with a retention time of 8.9 minutes. The samples were quantified against known concentrations of the TOB (calibration curve 6-120 µg/mL, R^2 = 0.9954, the limit of quantification 3 µg/mL).

The rate of TOB released was calculated as previously described,[25] using Higuchi (**Equation 1**) and plotting the square root of time against the total amount of TOB released. The slope of the plot is equal to the rate of release.[73, 74]

Equation 1: $Q = [D_m . C_d(2A - C_d)t]^{1/2}$

Where Q is the amount of drug released per unit matrix (mg/mL), D_m is the diffusion coefficient of the drug in the matrix, A is the initial amount of drug-loaded in the matrix, C_d is the solubility in the drug matrix, and t is time.

4.1.5. Deposition efficiency

The Aerogen® Pro (vibrating mesh nebulizer, Device Technologies, Medindie, SA, Australia) connected to a deposition device was used to aerosolize unformulated solutions of TOB and LCNPs loaded with TOB. The deposition device, described by Horstmann *et al.*[33] fitted into the well of a 24-well plate, ensuring the dose was deposited into a single well. Before use, the nebulizer was rinsed twice with 0.9% NaCl. Then each formulation of TOB was tested to ensure an even aerosol was produced. 100 µL of TOB as an unformulated solution, and in MO-LCNPs and PHY-LCNPs was nebulized into individual wells of a 24-well plate, containing 200 µL of

0.9% NaCl. The total antibiotic concentration was then determined from each well to calculate the total mass deposited. The nebulized samples were assessed for particle size and zeta potential, as described above.

For the nebulization samples and transport studies later described, TOB was quantified by liquid chromatography-tandem mass spectrometry (LC-MS) using a Dionex UltiMate 3000 Binary Rapid Separation LC System (Thermo Scientific, Waltham, MA, USA) coupled with a TSQ Quantum Access Max (QQQ, Thermo Scientific, USA) and a modified ion-pairing method. Before analysis, LCNPs were dissolved through mixing with 0.05% Triton X and then filtered using 4 mm Millex® syringe filters. The analytical column was a Zorbax Eclipse xdb C-18 column (5 µm, 50*4,6 mm, Agilent, USA) with C18 guard column. As a mobile phase, acetonitrile (eluent A) and water (eluent B), each supplemented with 0.1 % trifluoracetic acid, 0.1% heptafluorobutyric acid and 0.1% pentafluoropropionic acid were used. Samples were run with a flow of 0.7 mL/min, using a gradient of eluents A and B, starting with a ratio of 20:80 in the first minute. From 1 to 3.5 min, the ratio changed to 70:30 and was restored to 20:80 between 3.5 and 4.5 min. 3 µL of the samples were injected, and quantification was done by ESI+ and the SRM of the ion 468.184 →323.960.

4.2. Antimicrobial evaluations against planktonic P. aeruginosa

4.2.1. Minimum inhibitory concentration (MIC) determination

Standard micro-broth dilution assays assessed the antimicrobial activities of TOB, and CIP as unformulated solutions or loaded in the MO-LCNPs with planktonic *P. aeruginosa* in 96 well plates. A log-phase growth suspension of PAO1 (American Type Culture Collection, ATCC, Manassas, VA, USA) was diluted from an overnight culture to an OD600 of 0.01 (1×10^8 CFU/mL) in Luria-Bertani (LB, Gibco, ThermoFisher Scientific, Waltham, MA, United States) and added to the wells of the 96-well plate. The bacteria were diluted 1:1 with the serially diluted antibiotic, ranging from 0.125 – 128 µg/mL. As a control, the bacteria were 1:1 diluted

with 0.01 M PBS. After 18 h incubation at 37ºC, the inhibitory concentration was determined as the last clear well that had a comparable OD600 value to the sterile media control. Duplicate experiments were completed with four replicates each time.

4.2.2. Lipid-mixing assay to determine PAO1 fusion with LCNPs

The potential membrane fusion between LCNPs and single PAO1 cells was determined via a lipid-mixing assay as previously described by Sachetelli *et al.*[14] with Octadecyl Rhodamine B Chloride (R18, ThermoFisher Scientific, Waltham, MA, USA). This fluorophore self-quenches upon incorporation into membrane lipids.[75] Briefly, R18 tagged MO-LCNPs R18 or R18 unformulated were mixed with an overnight culture of PAO1 diluted to an OD_{600} of 0.01 and incubated at 37ºC. The fluorescent intensity of R18 was recorded using Inspire Multimode Plate reader (Perkin Elmer, ThermoFisher Scientific Waltham, MA, USA) at an excitation wavelength of 560 nm and emission at 590 nm every minute for 30 minutes. As a control, R18 MO-LCNPs and unformulated R18 were quenched by solubilization with 5% Triton X. Upon membrane fusion, the R18 probe is diluted across two membranes, corresponding to an increase in fluorescent intensity. Therefore, the maximum fluorescent intensity, subtracted from the background, was correlated to the maximum fluorescent intensity of R18 following solubilization with 5% Triton X, to determine the fusion efficiency between planktonic PAO1 and R18 tagged MO-LCNPs and the unformulated probe.

4.3. Antimicrobial evaluations against biofilm P. aeruginosa

4.3.1. In vitro MBEC antibiofilm assay

An MBEC Assay® (Innovotech, Edmonton, AB, Canada) was utilized as a simplified *in vitro* model to compare different formulations of antibiotics. An inoculum of PAO1 from a freshly streaked agar plate was incubated for 18 h in LB broth before dilution in sterile water to an OD600 of 0.50 ± 0.10. The bacterial suspension was further diluted 1:100 in LB broth

(equivalent to 2 x 10^8 CFU/mL), and 200 µL were transferred into wells of the MBEC Assay®. The pegs on the lid of the MBEC Assay® were submerged into the bacterial suspension, with column 12 containing sterile LB broth as a negative control. The plate was incubated at 37°C on a rotating gyrator for 24 h to form biofilm on the pegs.

After 24 h incubation at 37ºC, the peg lid was removed and transferred into another 96-well microtiter plate containing sterile water for 30 seconds before being transferred into a treatment plate. The peg lid in the treatment plate was incubated for 24 h at 37°C on the rotating gyrator. In the first study, the treatment plate contained various concentrations of three different types of formulation: (1) TOB or CIP as an unformulated solution, (2) TOB or CIP unformulated solution with no drug containing MO-LCNPs and (3) TOB or CIP loaded MO-LCNPs. Each formulation was prepared at a concentration of 1 µg/mL, 5 µg/mL, 15 µg/mL and 60 µg/mL TOB and 0.25 µg/mL, 1 µg/mL, 5 µg/mL and 15 µg/mL CIP, which was loaded into the LCNPs at different concentrations as previously described in order to achieve a uniform dose of 0.25 mg/mL MO. The respective controls included drug-free formulations of MO-LCNP at an equivalent lipid concentration and 0.9% NaCl, respectively.

In the second study, the treatment plate contained: 200 µL of TOB (15 µg/mL) as an unformulated solution, TOB formulated as MO-LCNPs and PHY-LCNPs, and TOB formulated as liposomes, all diluted 1:80 in LB broth. The final concentration of MO and PHY was 0.25 mg/mL, and for DSPC: DPPG, the concentration was 0.05 mg/mL.

After 24 h incubation, the peg lid was transferred to a fresh plate containing sterilized water to inhibit treatments. Individual pegs were removed from the lid with sterilized pliers and placed in 1 mL of sterile water in Eppendorf tubes. For each treatment, three pegs were collected individually and subjected to 2 cycles of bath sonication for 1 minute and vortex mixing for 30 seconds to dislodge and suspend the bacteria from the pegs. Serial dilutions and agar dilutions

were prepared, followed by enumeration by colony forming units (CFU). In addition to the three technical replicates, the assay was completed on three different occasions (biological replicates).

The biofilms formed were confirmed visually using scanning electron microscopy, as previously described.[76] Briefly, the bacteria grown on the pegs for 24 h were fixed with 2.5% glutaraldehyde (Sigma-Aldrich, St. Louis, MO, USA) for 30 mins, then 1% w/v osmium tetraoxide (Sigma-Aldrich, St. Louis, MO, USA) for 60 mins. The samples were then dehydrated in an ethanol series from 25% to 100% v/v and dried in hexamethyldisilazane (Sigma-Aldrich, St. Louis, MO, USA)) before mounting onto carbon tape and sputter-coated with 8.0 nm of gold. The images were obtained with a Zeiss Gemini 2 scanning electron microscope at an accelerating voltage of 2.0 kV.

4.3.2. Simple in vitro biofilm model

Biofilms were also formed in transparent, flat-bottom 96-well plates (Interpath Services Pty. Ltd., Heidelberg West, VIC, Australia), using the same bacterial suspension preparation as described above. Suspensions PAO1 (2 x 10^8 CFU/mL) in LB broth were incubated for 72 h at 37ºC to form biofilms on the bottom of the 96-well plates. Then, biofilms were gently washed twice with 0.9% NaCl before treatments were added as a suspension on top, and the plates were incubated for a further 24 h at 37ºC. In 200 µL LB broth, 15 µg/mL TOB as an unformulated solution was compared to when loaded in the MO-LCNPs (concentration 0.05 mg/mL). In addition, TOB MO-LCNPs with varied Pluronic® F-127 concentrations (i.e. 0%, 0.3% and 5% w/v) were also examined (constant MO-LCNPs concentration of 0.05 mg/mL). Following treatment incubations, the biofilms were scratched off the bottom of the wells and placed in microtubes that were vortexed for 10 mins to disrupt the biofilm. The bacterial suspensions were then serial diluted as previously described to quantify the CFU for each sample.

The biofilms were visualized via confocal microscopy using GFP tagged PAO1 (American Type Culture Collection, ATCC, Manassas, VA, USA) grown on sterile glass coverslips on the bottom of a 24-well plate (Interpath Services Pty. Ltd., Heidelberg West, VIC, Australia). After formation, the biofilms were washed and then fixed with formaldehyde (2% v/v, Sigma-Aldrich, St. Louis, MO, USA) for 20 mins. The coverslips were mounted onto a glass slide and imaged through confocal microscopy using a Zeiss Elyra PS. 1 Laser Scanning Confocal Microscope (Carl Zeiss Microscopy GmbH, Oberkochen, Germany).

4.3.3. Flow cell biofilm for laser scanning confocal microscopy

A two-channel transmission flow cell (Biosurface Technologies, Montana, US) attached to a reservoir bottle containing 1% sterile LB broth (pH 7.2) via a bubble trap was used similar to previous setups.[9, 77] An overnight culture of PAO1 GFP strain was diluted in 1% LB broth (pH 7.2) to an OD of 0.01 and injected into the flow cell, and the flow was stopped. The bacteria were allowed to attach to the glass support for 1 h before the flow (0.4 mL/min) was resumed. Biofilms were grown at 37ºC for three days.

15 µg/mL of Cy5 TOB or 5 µg/mL Cy5 CIP (Biosynthesis, Texas, US, Lot number: SP2260-1,-2) dissolved in 0.9% NaCl or loaded as previously described in MO-LCNPs (0.05 mg/mL) was injected into individual channels of the flow cell and imaged via laser scanning microscopy (LSM700, Zeiss, Oberkochen, Germany) at 0.5, 1 and 2 h following injection. ZenBlue and ImageJ software were used to complete the analysis of z-stack images.

4.4. Cell toxicity

The cellular toxicity of MO- and PHY-LCNPs was assessed over 24 h in the cystic fibrosis bronchial epithelium cell line (CFBE41o-) via lactate dehydrogenase (LDH) release from the cells. LDH is an enzyme that is released upon cell lysis, indicating a direct measure for cell

death.[78] CFBE41o- cell line (Gruenert Cell Line Distribution Program) were grown in minimum essential medium (MEM, Gibco, ThermoFisher Scientific, Waltham, MA, USA) supplemented with 10% fetal calf serum (FCS, Lonza), 1% non-essential amino acids (NEAA 100x, Gibco) and 0.6 mg/mL D-(+)-glucose (Sigma Aldrich, St. Louis, MO, USA). The cells were passaged at 0.2 x 10^6 cells in a T75 flask (ThermoFisher Scientific, Waltham, MA, USA) once a week, refreshing the media every 2-3 days. For the toxicity assays, cells were seeded at 0.02 x 10^6 cells/well in a 96 well plate in MEM media (p 4.86-4.86). The cells were incubated at 37ºC at 5% CO_2 for 18 h to allow them to adhere. Thereafter, the cells were washed once with PBS, and the respective treatments were added. 0.01 – 10 mg/mL of MO- and PHY-LCNPs loaded with and without TOB were prepared from stocks of LCNPs diluted in MEM media. Non-treated cells and cells treated with 5% Triton X were used as respective positive and negative controls. The plates were re-incubated for 24 h. After 24 h, the 96-well plates are centrifuged at 300 x g for 10 minutes. 100 µL of the supernatant is transferred to a new 96 well plate, and each well is mixed with 100 µL of Cytotoxicity Detection Kit (LDH) (Roche, Sigma Aldrich, St. Louis, MO, USA)), as per the manufacture's instruction. After 5-minute incubation at room temperature, the LDH release was assessed by subtracting the absorbance of the sample at 492 nm from the living control absorbance. The % viability was calculated by subtracting the sample's LDH released from the LDH released from Triton X treated wells(dead cell control), divided by the LDH release of the Triton X treated well, multiplied by 100. Four individual experiments were carried out, each with 2 replicates, providing a total of 8 replicates.

4.5. Chronic infection model: CFBE41o- and PAO1

The chronic infection model was developed by Horstmann *et al.* (manuscript in preparation), which cultures *P. aeruginosa* biofilm on top of the bronchial CF epithelium cells (CFBE41o-) at an air-liquid interface. It is a biologically relevant model that resembles the infected lungs of CF patients.

CFBE41o- cell line was seeded at 0.05 x 10^6 cells per well on Transwell® inserts (Corning®, Lot #29819052-89 Sigma Aldrich, St. Louis, MO, USA,) at the liquid-liquid interface (500 µL apical and 1500 µL basolateral) on day 0. On day 3, the apical side media was removed, and the basolateral side was replaced with 500 µL of media. On day 7, the transepithelial electrical resistance (TEER) was measured by a voltammeter equipped with STX2 chopstick manual electrodes (EVOM, World Precision Instruments, USA). Cells at the air-liquid interface were first pre-incubated with 500 µL and 1500 µL of MEM media (apical and basolateral, respectively) for 1.5 h at 37ºC. Three measurements were taken at 37ºC in different positions and averaged for each time point per well.

From an overnight culture, PAO1 was diluted in 500 µL of M63 media to an OD of 0.01 in 24 well plates and incubated for 72 h at 37ºC to form biofilms. Breath seals were used to permit gas exchange during the 72 h incubation period. After 72 h, the biofilms were washed with 500 µL PBS to remove detached planktonic bacteria. Then, using 200 µL of M63 buffer, the biofilms were scraped off the bottom of the 24-well plate using a 1 mL pipette tip and transferred on top of the CFBE41o- cell line in the apical compartment of the Transwells® on day 7. After 1 h incubation, the supernatant was removed as the biofilm has settled onto the cells. This maintained the model at the air-liquid interface.

Using the Aerogen® Pro (vibrating mesh nebulizer) and deposition device, the treatments were then nebulized on top of the biofilm and CFBE41o- cell layer, as aforementioned. An unformulated solution of TOB and MO-LCNPs TOB were dosed at 12 µg, equivalent to 100 µL of 3.32 mg/mL for unformulated TOB and 2.50 mg/mL for MO-LCNPs TOB. The treatments were prepared by diluting the stock solution/LCNPs suspension to the required concentration in KRB buffer. Each time the nebulizer was first rinsed with KRB buffer and the Transwell® to be dosed was transfer to a clean 12 well plate. The treatment was nebulized following a 30-second deposition waiting time. After all treatments were dosed, the

Transwells® were replaced to their original well that included fresh MEM media supplemented with 1% arginine basolateral (500 µL) and the plates were incubated for the required time at 37ºC.

At the time points of 24 h, 48 h, and 72 h different readouts were obtained, including bacterial counts, the viability of cells, barrier integrity (via sodium fluorescein transport) and TOB transport.

Following 24 h post the second or third dose (at 48 h and 72 h, respectively), the basolateral cell medium was removed and replaced with fresh media. The samples were kept for an extra two days, enumerating the CFU and cell viability at 24 h time points. In three independent replicates, each repeat involved a total of nine samples for each treatment which were split into three groups to determine the bacterial load and cell viability at 48 h and 72 h post-dose and a separate group was processed for confocal microscopy.

4.5.1. Colony Forming Unit (CFU) assessment

Bacteria were enumerated through adding 500 µL of sterile, cold Milli-Q water to the apical and basolateral compartment. The cold water lysed the cells, and after 10 minutes, a pipette tip was used to scratch off the remaining biofilm and transfer all the contents of the apical compartment into an Eppendorf tube.[28] To ensure all bacteria were removed, a further 500 µL of PBS + 0.05 % Tween® 80 (Sigma-Aldrich, St. Louis, MO, USA) was added to repeat the apical compartment wash and was then transferred into the same Eppendorf tube. Serial dilutions up to 10^{10} were performed, and 20 µL of each dilution was plated onto LB agar plates. The plates were incubated for 18 h at 30ºC before the colonies of bacteria were counted.

4.5.2. Toxicity assessment

Cell viability was assessed by taking the contents of the basolateral compartment media and reacting it with a Cytotoxicity Detection Kit (LDH) to determine the amount of LDH released, as aforementioned. 200 µL of the basolateral media was taken and centrifuged at 300 x g for 10 mins. 100 µL of the supernatant was mixed with 100 µL of the reaction solution, as per manufactures instructions. LDH release was measured after a 5-minute incubation at room temperature using a plate reader at an absorbance of 492 nm.

4.5.3. Barrier integrity

The barrier integrity of the CFBE41o- cell line cultured on the Transwell® supports was determined by both TEER (as aforementioned) and sodium fluorescein transport.[79] Due to the variation in TEER measurements, sodium fluorescein transport provides a direct measurement of the tight junctions. On day 7 (4 days after cells are transferred to ALI), cells were incubated basolaterally with 1.7 mL KRB buffer and apically with 520 µL of 10 µg/mL sodium fluorescein (Sigma-Alrich, St. Louis, MO, USA) (in KRB) with or without 16 mM ethylenediaminetetraacetic acid (EDTA, Sigma-Aldrich, St. Louis, MO, USA). EDTA disrupts the tight junctions of a cell barrier. The initial measurement was taken via removing 20 µL from the apical side and 200 µL from the basolateral compartment. At 30-minute intervals, 200 µL samples were taken from the basolateral compartment and replaced with fresh KRB. During the transport study, the plates were incubated at 37ºC on an MTS orbital shaker (150 rpm, IKA, Germany). The samples were then measured and compared to a standard curve via fluorescent spectroscopy (Tecan® plate reader, Tecan Deutschland GmbH, Germany) at excitation and an emission wavelength of 530 nm 488 nm, respectively. The amount of sodium fluorescein transported was plotted against time, where the slope was taken to calculate the apparent permeability coefficients (Papp).[80, 81]

Equation 2: $P_{app} = \frac{dQ}{dt} \; x \; \frac{1}{A \times C_0}$

Where the slope is dQ/dt, a is the area of the Transwell® insert and C_0 is the initial concentration of sodium fluorescein in the apical compartment.

4.5.4. Tobramycin transport

After TOB treatments were nebulized, at 5, 15, 30, 60, 120, 240 and 1440 minutes, 100 µL sample was taken from the basolateral compartment (supplemented with KRB for transport-specific studies) and replaced with fresh KRB media. The sample was then filtered through 4 mm Millex® syringe filters (Merck, Darmstadt, Germany) before LC-MS/MS analysis, as described above, to quantify the transport of TOB.

4.5.5. Laser scanning confocal microscopy

At 0, 4, 24 and 48 h post-PAO1 tagged with GFP infection, CFBE41o- cells were fluorescently stained with 5 µg/mL Wheat Germ Agglutinin, Alexa Fluor™ 633 Conjugate (Thermo Fisher Scientific, Waltham, MA, US) and 0.05 µg/mL DAPI (Sigma-Aldrich, St. Louis, MO, USA) before fixation with 3% formaldehyde. Samples were either treated with KRB, TOB or TOB MO-LCNPs (tagged with R18). Samples were imaged via laser scanning confocal microscopy using Zeiss LSM700 Confocal Microscope (Carl Zeiss AG, Oberkochen, Germany), maintaining the same laser power, gain and offset settings.

4.6. Statistical analysis

Data are reported as mean ± standard deviation. One-way and two-way analysis of variance (ANOVA) assessed the difference in the deposition efficiency and antimicrobial activities of various formulations (as described in figures). Statistical significance was evaluated at the 95% confidence interval. All tests were performed using GraphPad Prism (version 7.00 for Windows; GraphPad Software, La Jolla, CA).

Supporting Information

Supporting Information is available from the Wiley Online Library or from the author.

Figure 1: CFBE41o- cell toxicity to monoolein- and phytantriol- liquid crystalline nanoparticles; Figure 2: Chronic infection model treated with nebulized TOB as an unformulated solution or loaded in monoolein liquid crystalline nanoparticles, *P. aeruginosa* load and CFBE41o- viability at 24 h and 48 h; Figure 3: Representative confocal microscopy images of chronic infection model after unformulated TOB nebulized treatments

Acknowledgements

We sincerely thank the technical assistance of P. Paul, Dr A. Boese, P. König, and J. Westhues at the Helmholtz Institute for Pharmaceutical Research Saarland and A. Kral, A. Wignall and S. Hodby from the University of South Australia. CRT is grateful for scholarships and funding support from the Australia Government Research Training Stipend and the Department of Education and Training Endeavour Postgraduate Leadership Award, Gould Experimental Grant Encouragement Award and BUPA Health Research. NT is supported by a Mid-Career Fellowship from The Hospital Research Foundation.

Received: ((will be filled in by the editorial staff))

Revised: ((will be filled in by the editorial staff))

Published online: ((will be filled in by the editorial staff))

References

1. Fleming, D.; Rumbaugh, K. P., *Microorganisms* **2017,** *5* (2).
2. Costerton, J. W.; Lewandowski, Z.; Caldwell, D. E.; Korber, D. R.; Lappin-Scott, H. M., *Annu. Rev. Microbiol.* **1995,** *49*, 711-45.
3. Govan, J. R.; Deretic, V., *Microbiol. Mol. Biol. Rev.* **1996,** *60* (3), 539-574.

4. Davies, J. C.; Alton, E. W. F. W.; Bush, A., *BMJ [Br. Med. J.]* **2007,** *335* (7632), 1255-1259.
5. Flume, P. A.; Peter J. Mogayzel, J.; Robinson, K. A.; Goss, C. H.; Rosenblatt, R. L.; Kuhn, R. J.; Marshall, B. C.; Committee*, a. t. C. P. G. f. P. T., *Am. J. Respir. Crit. Care Med.* **2009,** *180* (9), 802-808.
6. Hoiby, N.; Bjarnsholt, T.; Moser, C.; Bassi, G. L.; Coenye, T.; Donelli, G.; Hall-Stoodley, L.; Hola, V.; Imbert, C.; Kirketerp-Moller, K.; Lebeaux, D.; Oliver, A.; Ullmann, A. J.; Williams, C.; Biofilms, E. S. G. f.; Consulting External Expert Werner, Z., *Clin. Microbiol. Infect.* **2015,** *21 Suppl 1*, S1-25.
7. Müller, L.; Murgia, X.; Siebenbürger, L.; Börger, C.; Schwarzkopf, K.; Sewald, K.; Häussler, S.; Braun, A.; Lehr, C.-M.; Hittinger, M.; Wronski, S., *J. Antimicrob. Chemother.* **2018,** *73* (10), 2762-2769.
8. Boge, L.; Murgia, X.; Hittinger, M.; Siebenbuerger, L.; Boerger, C.; Groß, H.; Braun, A.; Sewald, K.; Lehr, C.-M.; Wronski, S., *Eur. Respir. J.* **2017,** *50* (suppl 61), PA1344.
9. Tseng, B. S.; Zhang, W.; Harrison, J. J.; Quach, T. P.; Song, J. L.; Penterman, J.; Singh, P. K.; Chopp, D. L.; Packman, A. I.; Parsek, M. R., *Environ Microbiol* **2013,** *15* (10), 2865-78.
10. Beringer, P. M.; Vinks, A. A.; Jelliffe, R. W.; Shapiro, B. J., *Antimicrob. Agents Chemother.* **2000,** *44* (4), 809-813.
11. Smyth, A. R., *J. R. Soc. Med.* **2010,** *103* (1_suppl), 3-5.
12. Forier, K.; Raemdonck, K.; De Smedt, S. C.; Demeester, J.; Coenye, T.; Braeckmans, K., *J. Controlled Release* **2014,** *190*, 607-623.
13. Ho, D.-K.; Murgia, X.; De Rossi, C.; Christmann, R.; Hüfner de Mello Martins, A. G.; Koch, M.; Andreas, A.; Herrmann, J.; Müller, R.; Empting, M.; Hartmann, R. W.; Desmaele, D.; Loretz, B.; Couvreur, P.; Lehr, C.-M., *Angew. Chem. Int.* **2020,** *59* (26), 10292-10296.
14. Sachetelli, S.; Khalil, H.; Chen, T.; Beaulac, C.; Senechal, S.; Lagace, J., *Biochim. Biophys. Acta* **2000,** *1463* (2), 254-66.
15. Shirley, M., *Drugs* **2019,** *79* (5), 555-562.
16. Zhang, J.; Leifer, F.; Rose, S.; Chun, D. Y.; Thaisz, J.; Herr, T.; Nashed, M.; Joseph, J.; Perkins, W. R.; DiPetrillo, K., *Front. Microbiol.* **2018,** *9*, 915-915.
17. Bangham, A. D.; Horne, R. W., *J. Mol. Biol.* **1964,** *8* (5), 660-IN10.
18. Drummond, C. J.; Fong, C., *Curr. Opin. Colloid Interface Sci.* **1999,** *4* (6), 449-456.
19. Tan, A.; Hong, L.; Du, J. D.; Boyd, B. J., *Adv. Sci.* **2019,** *6* (3), 1801223.
20. Clogston, J.; Caffrey, M., *J. Controlled Release* **2005,** *107* (1), 97-111.
21. Mezzenga, R.; Seddon, J. M.; Drummond, C. J.; Boyd, B. J.; Schröder-Turk, G. E.; Sagalowicz, L., *Adv. Mater.* **2019,** *31* (35), 1900818.
22. Rizwan, S. B.; Boyd, B. J.; Rades, T.; Hook, S., *Expert Opin. Drug Deliv.* **2010,** *7* (10), 1133-44.
23. Luzzati, V.; Tardieu, A.; Gulik-Krzywicki, T.; Rivas, E.; Reiss-Husson, F., *Nature* **1968,** *220* (5166), 485-488.
24. Scriven, L. E., *Nature* **1976,** *263* (5573), 123-125.
25. Thorn, C. R.; Clulow, A. J.; Boyd, B. J.; Prestidge, C. A.; Thomas, N., *J. Controlled Release* **2020,** *319*, 168-182.
26. Lavelle, G. M.; White, M. M.; Browne, N.; McElvaney, N. G.; Reeves, E. P., *Biomed Res. Int.* **2016,** *2016*, 5258727.
27. Costa, A.; de Souza Carvalho-Wodarz, C.; Seabra, V.; Sarmento, B.; Lehr, C.-M., *Acta Biomater.* **2019,** *91*, 235-247.

28. Montefusco-Pereira, C. V. H., Justus C.; Ebensen, Thomas; Beisswenger, Christoph; Bals, Robert; Guzmán, Carlos A.; Schneider-Daum, Nicole; Carvalho-Wodarz, Cristiane de Souza; Lehr, Claus-Michael, *JoVE* **2020,** (160), e61069.
29. Artzy-Schnirman, A.; Lehr, C.-M.; Sznitman, J., *Expert Opin. Drug Deliv.* **2020**, 1-5.
30. Bjarnsholt, T.; Alhede, M.; Alhede, M.; Eickhardt-Sørensen, S. R.; Moser, C.; Kühl, M.; Jensen, P.; Høiby, N., *Trends Microbiol.* **2013,** *21* (9), 466-74.
31. Higuchi, W. I. Diffusional Models Useful in Biopharmaceutics. Drug Release Rate Processes *J. Pharm. Sci.* [Online], 1967, p. 315-324. http://dx.doi.org/10.1002/jps.2600560302.
32. Lagacé, J.; Dubreuil, M.; Montplaisir, S., *J. Microencapsulation* **1991,** *8* (1), 53-61.
33. Horstmann, J. C.; Thorn, C. R.; Carius, P.; Graef, F.; Murgia, X.; de Souza Carvalho-Wodarz, C.; Lehr, C.-M., *Front. Bioeng. Biotechnol.* **2021,** *Under Review*.
34. Dailey, L. A.; Schmehl, T.; Gessler, T.; Wittmar, M.; Grimminger, F.; Seeger, W.; Kissel, T., *J. Controlled Release* **2003,** *86* (1), 131-144.
35. Moore, R. D.; Smith, C. R.; Lietman, P. S., *Am. J. Med.* **1984,** *77* (4), 657-62.
36. Coulthard, K. P.; Peckham, D. G.; Conway, S. P.; Smith, C. A.; Bell, J.; Turnidge, J., *J. Cystic Fibrosis* **2007,** *6* (2), 125-130.
37. Begg, E. J.; Barclay, M. L.; Kirkpatrick, C. J. M., *Br. J. Clin. Pharmacol.* **1999,** *47* (1), 23-30.
38. Novartis, P. C., TOBI PODHALER- Tobramycin Capsule In *Product Information*, Revised 07/2020.
39. Thorn, C. R.; Thomas, N.; Boyd, B. J.; Prestidge, C. A., *Drug Delivery Transl. Res.* **2021**, 1-27.
40. Beaulac, C.; Clément-Major, S.; Hawari, J.; Lagacé, J., *Antimicrob. Agents Chemother.* **1996,** *40* (3), 665-669.
41. Halwani, M.; Mugabe, C.; Azghani, A. O.; Lafrenie, R. M.; Kumar, A.; Omri, A., *J. Antimicrob. Chemother.* **2007,** *60* (4), 760-769.
42. Alhariri, M.; Majrashi, M. A.; Bahkali, A. H.; Almajed, F. S.; Azghani, A. O.; Khiyami, M. A.; Alyamani, E. J.; Aljohani, S. M.; Halwani, M. A., *Int. J. Nanomedicine* **2017,** *12*, 6949-6961.
43. Waters, V.; Ratjen, F., *Expert review of respiratory medicine* **2014,** *8* (4), 401-9.
44. Hinton, T. M.; Grusche, F.; Acharya, D.; Shukla, R.; Bansal, V.; Waddington, L. J.; Monaghan, P.; Muir, B. W., *Toxicol Res-Uk* **2014,** *3* (1), 11-22.
45. Dyett, B. P.; Yu, H.; Strachan, J.; Drummond, C. J.; Conn, C. E., *Nat. Commun.* **2019,** *10* (1), 4492.
46. Barriga, H. M. G.; Holme, M. N.; Stevens, M. M., *Angew. Chem.* **2018,** *131* (10), 2984-3006.
47. Rattanapak, T.; Young, K.; Rades, T.; Hook, S., *J. Pharm. Pharmacol.* **2012,** *64* (11), 1560-9.
48. Mendrok-Edinger C; Mongiat, S. R., T; Schlifke-Poschalko, A Use of Phytantriol as an Antimicrobial Agent. EP3485869A1, 2017.
49. Messiaen, A.-S.; Forier, K.; Nelis, H.; Braeckmans, K.; Coenye, T., *PLOS ONE* **2013,** *8* (11), e79220.
50. Meers, P.; Neville, M.; Malinin, V.; Scotto, A. W.; Sardaryan, G.; Kurumunda, R.; Mackinson, C.; James, G.; Fisher, S.; Perkins, W. R., *J. Antimicrob. Chemother.* **2008,** *61* (4), 859-868.
51. Ceri, H.; Olson, M. E.; Stremick, C.; Read, R. R.; Morck, D.; Buret, A., *J. Clin. Microbiol.* **1999,** *37* (6), 1771-1776.
52. Schneider, C. S.; Xu, Q.; Boylan, N. J.; Chisholm, J.; Tang, B. C.; Schuster, B. S.; Henning, A.; Ensign, L. M.; Lee, E.; Adstamongkonkul, P.; Simons, B. W.; Wang, S.-Y. S.; Gong, X.; Yu, T.; Boyle, M. P.; Suk, J. S.; Hanes, J., *Sci. Adv.* **2017,** *3* (4), e1601556.

53. Yang, M.; Lai, S. K.; Wang, Y. Y.; Zhong, W.; Happe, C.; Zhang, M.; Fu, J.; Hanes, J., *Angew. Chem. Int.* **2011,** *50* (11), 2597-600.
54. Suk, J. S.; Xu, Q.; Kim, N.; Hanes, J.; Ensign, L. M., *Adv Drug Deliv Rev* **2016,** *99* (Pt A), 28-51.
55. Yu, T.; Wang, Y.-Y.; Yang, M.; Schneider, C.; Zhong, W.; Pulicare, S.; Choi, W.-J.; Mert, O.; Fu, J.; Lai, S. K.; Hanes, J., *Drug Delivery Transl. Res.* **2012,** *2* (2), 124-128.
56. Thornton, D. J.; Sheehan, J. K., *Proc. Am. Thorac. Soc.* **2004,** *1* (1), 54-61.
57. Flemming, H.-C.; Wingender, J.; Szewzyk, U.; Steinberg, P.; Rice, S. A.; Kjelleberg, S., *Nat. Rev. Microbiol.* **2016,** *14*, 563–575.
58. Dong, Y.-D.; Larson, I.; Barnes, T. J.; Prestidge, C. A.; Boyd, B. J., *ACS Appl. Mater. Interfaces* **2011,** *3* (5), 1771-1780.
59. De Leo, L.; Di Toro, N.; Decorti, G.; Malusà, N.; Ventura, A.; Not, T., *Antimicrob. Agents Chemother.* **2010,** *54* (4), 1644-1646.
60. Zambito, Y.; Zaino, C.; Di Colo, G., *Eur. J. Pharm. Biopharm.* **2006,** *64* (1), 16-25.
61. Cooney, G. F.; Lum, B. L.; Tomaselli, M.; Fiel, S. B., *J. New Drugs* **1994,** *34* (3), 255-259.
62. Valcke, Y.; Pauwels, R.; Van der Straeten, M., *Eur. Respir. J.* **1990,** *3* (6), 715-722.
63. Touw, D.; Jacobs, F.; Brimicombe, R.; Heijerman, H.; Bakker, W.; Briemer, D., *Antimicrob. Agents Chemother.* **1997,** *41* (1), 184-187.
64. Ehrhardt, C.; Collnot, E.-M.; Baldes, C.; Becker, U.; Laue, M.; Kim, K.-J.; Lehr, C.-M., *Cell Tissue Res.* **2006,** *323* (3), 405-415.
65. Mulcahy, L. R.; Burns, J. L.; Lory, S.; Lewis, K., *J. Bacteriol.* **2010,** *192* (23), 6191-6199.
66. Akiyama, T.; Williamson, K. S.; Schaefer, R.; Pratt, S.; Chang, C. B.; Franklin, M. J., *PNAS* **2017,** *114* (12), 3204-3209.
67. Wood, T. K.; Knabel, S. J.; Kwan, B. W., *Appl. Environ. Microbiol.* **2013,** *79* (23), 7116-7121.
68. Mojsoska, B.; Cameron, D. R.; Bartell, J. A.; Haagensen, J. A. J.; Sommer, L. M.; Lewis, K.; Molin, S.; Johansen, H. K., *bioRxiv* **2019**, 561589.
69. Gonzalez, L. S., 3rd; Spencer, J. P., *Am. Fam. Physician* **1998,** *58* (8), 1811-20.
70. Ratjen, F.; Munck, A.; Kho, P.; Angyalosi, G., *Thorax* **2010,** *65* (4), 286-91.
71. Allison, K. R.; Brynildsen, M. P.; Collins, J. J., *Nature* **2011,** *473* (7346), 216-220.
72. Russ, H.; McCleary, D.; Katimy, R.; Montana, J. L.; Miller, R. B.; Krishnamoorthy, R.; Davis, C. W., *J. Liq. Chromatogr. Relat. Technol.* **2006,** *21* (14), 2165-2181.
73. Ho, N.; Turi, J.; Shipman Jr, C.; Higuchi, W., *J. Theor. Biol.* **1972,** *34* (3), 451-467.
74. Bisset, N. B.; Boyd, B. J.; Dong, Y. D., *Int. J. Pharm.* **2015,** *495* (1), 241-248.
75. Hoekstra, D.; de Boer, T.; Klappe, K.; Wilschut, J., *Biochemistry* **1984,** *23* (24), 5675-81.
76. Thorn, C. R.; Prestidge, C. A.; Boyd, B. J.; Thomas, N., *ACS Appl. Bio Mater.* **2018,** *1* (2), 281-288.
77. Christensen, B. B.; Sternberg, C.; Andersen, J. B.; Palmer, R. J., Jr.; Nielsen, A. T.; Givskov, M.; Molin, S., *Methods Enzymol.* **1999,** *310*, 20-42.
78. Kumar, P.; Nagarajan, A.; Uchil, P. D., *Cold Spring Harb. Protoc.* **2018,** *2018* (6).
79. Molenda, N.; Urbanova, K.; Weiser, N.; Kusche-Vihrog, K.; Günzel, D.; Schillers, H., *PLOS ONE* **2014,** *9* (6), e100621.
80. Ma, B.; Wang, J.; Sun, J.; Li, M.; Xu, H.; Sun, G.; Sun, X., *Int. J. Clin. Exp. Pathol.* **2014,** *7* (5), 1957-1966.
81. Hubatsch, I.; Ragnarsson, E. G. E.; Artursson, P., *Nat. Protoc.* **2007,** *2* (9), 2111-2119.

ToC figure

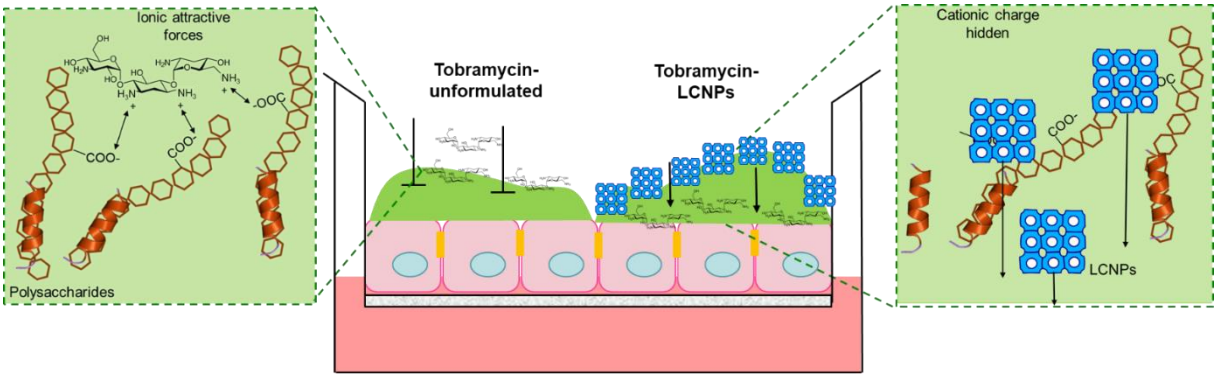
Ionic attractive forces
Polysaccharides
Tobramycin-unformulated
Tobramycin-LCNPs
Cationic charge hidden
LCNPs

Supporting Information

Tobramycin liquid crystalline nanoparticles eradicate cystic fibrosis-related Pseudomonas aeruginosa biofilms

Chelsea R. Thorn [A,B,C], Cristiane de Souza Carvalho-Wodarz [D], Justus C. Horstmann [D,E], Claus-Michael Lehr [D,E], Clive A. Prestidge [A,C] and Nicky Thomas [A,B,C]∗

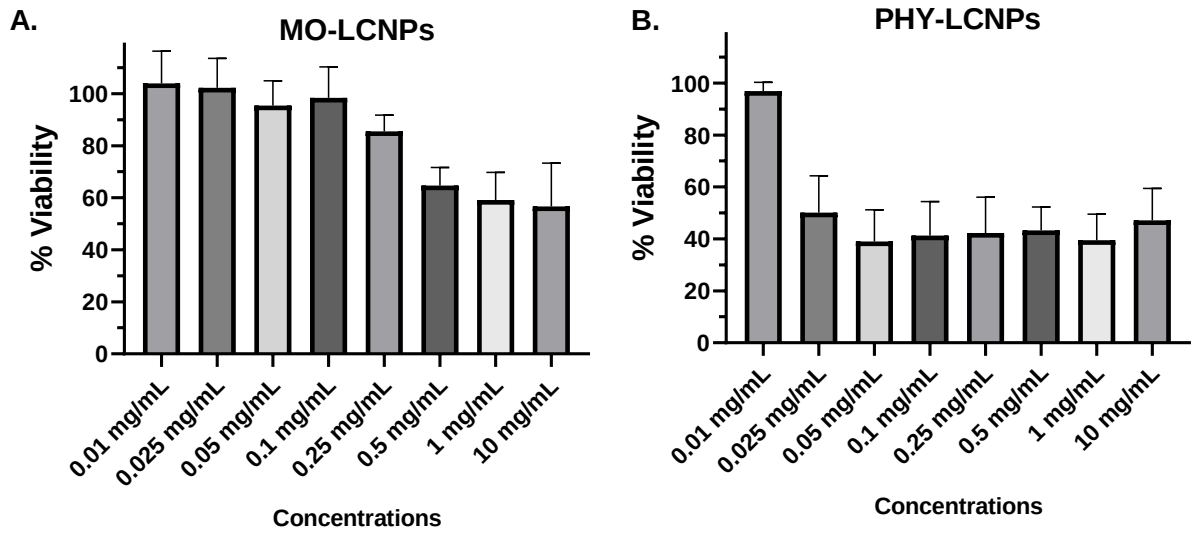

Supplementary Figure 8. Percentage of CFBE41o- cells (P 4.85, P 4.86) that were viable compared to incubation 5% Triton X, after treatment with varying concentrations of (A) MO-LCNPs and (B) PHY-LCNPs. CFBE41o- seeded 0.2 x 106 cells/well. Data represented as mean ± standard deviation, n = 8 (4 independent experiments).

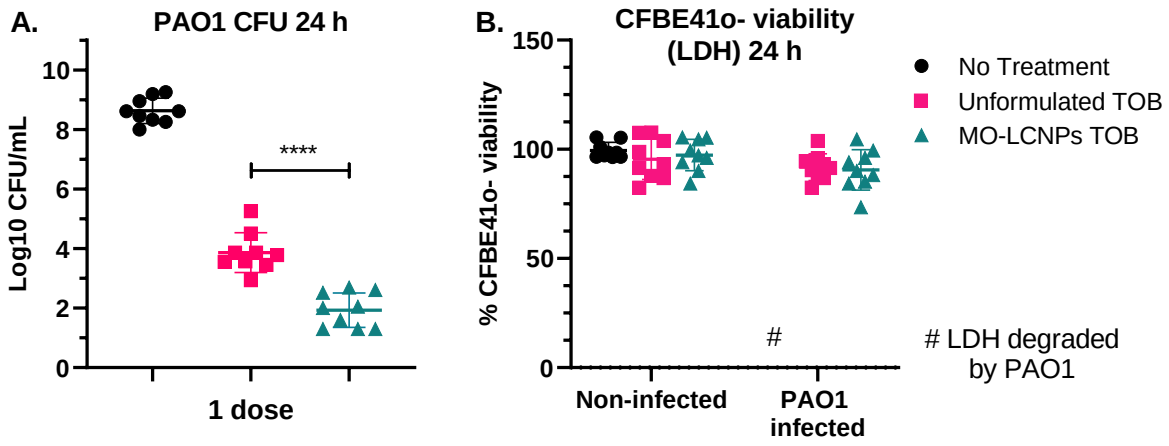

*Supplementary Figure 9. CFBE41o- (p 4.83, 4.85, p 4.87) 0.05 x 10^6 cells/well infected with PAO1 biofilm, following 24 h after nebulised treatment with 12 µg of unformulated tobramycin or 12 µg of MO-LCNPs (MO = 0.025 mg/mL) using the Aerogen® Pro (vibrating mesh nebuliser) + nebulisation chamber. A. total amount of PAO1 remaining after 24 h treatment and B. CFBE41o- viability assessed via LDH assay compared to cells treated with 5% Triton X. Data represented as mean ± standard deviation, n = 9 (3 independent experiments), one-way ANOVA with Tukey multiple comparison test **** = P < 0.0001*

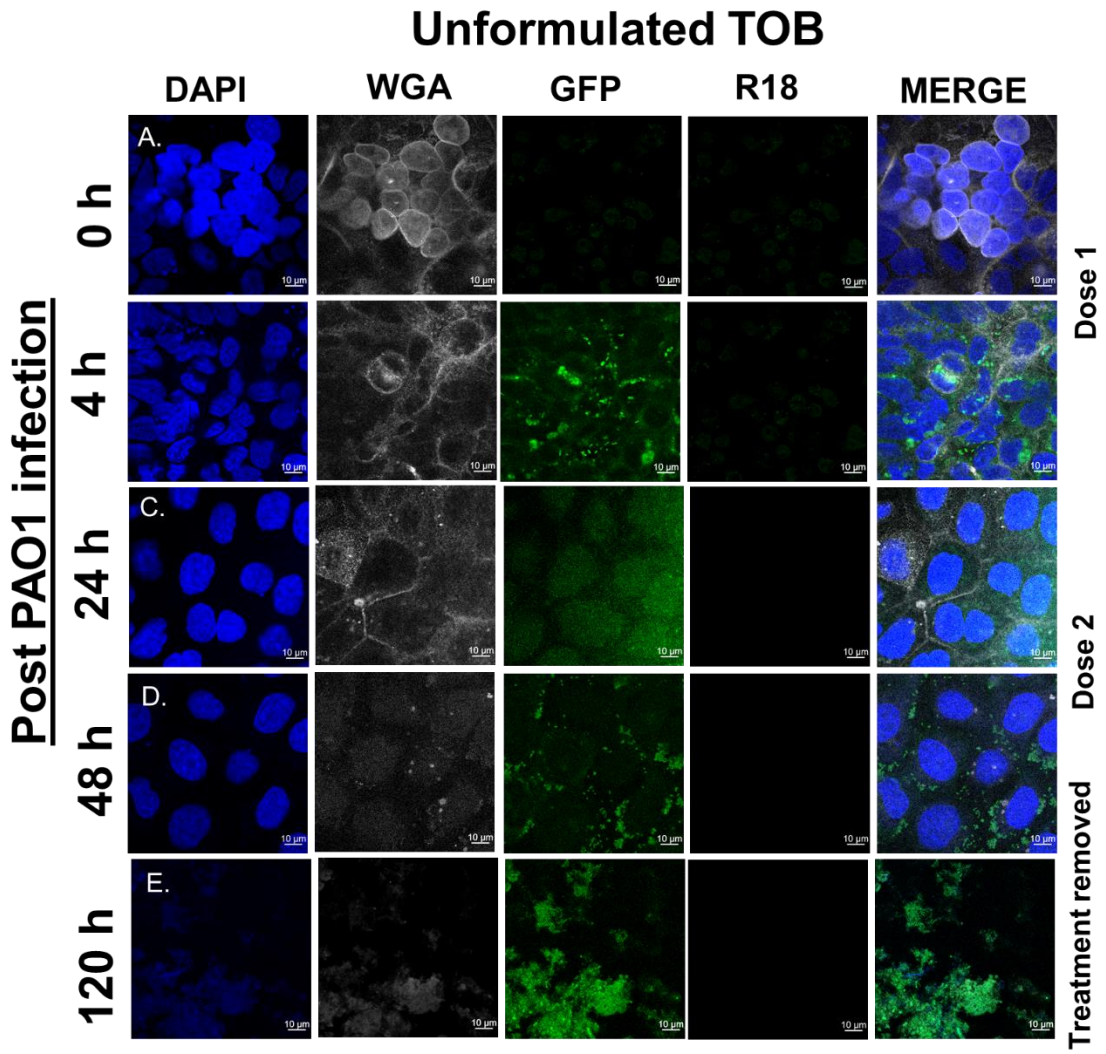

Supplementary Figure 10. Representative splits and merged confocal microscopy images of; A. CFBE41o- cells (nuclei stained with DAPI, WGA Alexa Fluoro 633 stained membranes) with no treatment, B.-E. are PAO1 (GFP-tagged) infected CFBE41o- cells at 4 h, 24 h, 48 h and 120 h post-infection following nebulization with unformulated TOB at 1 h and 24 h post-infection. The unformulated TOB was then removed via refreshing the basolateral medium at 48 h post-infection, and the cells were kept for an extra 72 h.